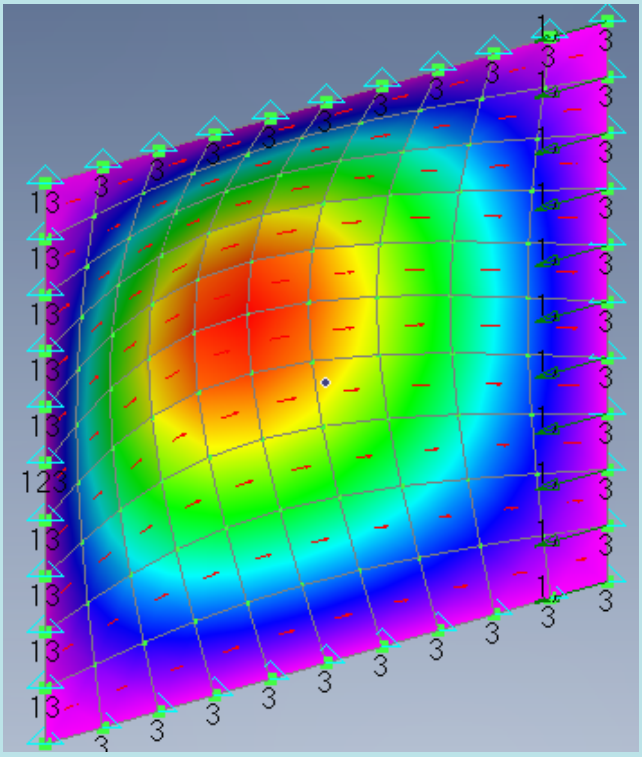

CA II with Matlab/Femap

Aerospace Structures Project (PART II)

Antonio Carotenuto

A.A 2024-2025

Contents

List of Figures

Chapter 1

Effect of Hole Drilling and Stress Concentration Factor

1.1 Introduction

The presence of a geometric discontinuity within a component, such as a hole, modifies the distribution of surrounding stresses, causing an increase in the maximum stress in that area. This phenomenon can be explained by considering that the density of stress flow lines is directly proportional to the stress intensity itself. In other words, when there is a discontinuity, like a hole, the flow lines tend to concentrate more around the affected area, causing an increase in stress in the immediate vicinity of the discontinuity, as shown in Fig.1.1.

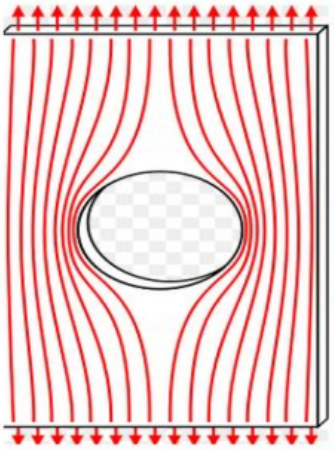

Figure 1.1 Stress flow lines around a hole

To describe this phenomenon, the quantity K_t, known as the stress concentration factor (or notch coefficient), is introduced and defined as:

$$K_t = \frac{\sigma_{\max}}{\sigma_0} \tag{1.1}$$

where σ_{max} is the maximum value that the stress assumes in the vicinity of the discontinuity, while σ_0 is the asymptotic value ideally reached at an infinite distance from it. In some particular cases, it is possible to express the concentration factor in analytical form, but generally, this can only be obtained numerically. Under the assumptions of:

- a plate made of metallic material;
- an elliptical hole;
- semi-axes a and b of the hole being very small compared to the plate dimensions;
- the hole being sufficiently far from the plate edges

(as in Fig.2.1), the analytical solution can be expressed as:

$$K_t = 1 + 2\frac{a}{b} \tag{1.2}$$

From this expression, we also derive that for a circular hole (a=b), K_t=3. It is also observed that ideally, as b $\rightarrow$ 0, $K_t \rightarrow \infty$. In reality, the analytical solution is valid as long as the mechanical behavior of the material is linear; when the stress around the hole becomes very large, the material plasticizes, and therefore the stress concentration factor does not go to infinity.

In the case of composite materials, if the hole is circular, small in size compared to the plate dimensions, and far from the edges, then the following expression for K_t can be used:

$$K_t = 1 + \sqrt{\frac{2}{A_{22}}(\sqrt{A_{11}A_{22}} - A_{12} + \frac{A_{11}A_{22} - A_{12}^2}{2A_{66}})} \tag{1.3}$$

and the stress distribution σ_x along the plate can be obtained using the following expression:

$$\sigma_x(0, y) = \frac{\sigma_0}{2}\left(2 + \left(\frac{R}{y}\right)^2 + 3\left(\frac{R}{y}\right)^4 - (K_t - 3)\left(5\left(\frac{R}{y}\right)^6 - 7\left(\frac{R}{y}\right)^8\right)\right) \tag{1.4}$$

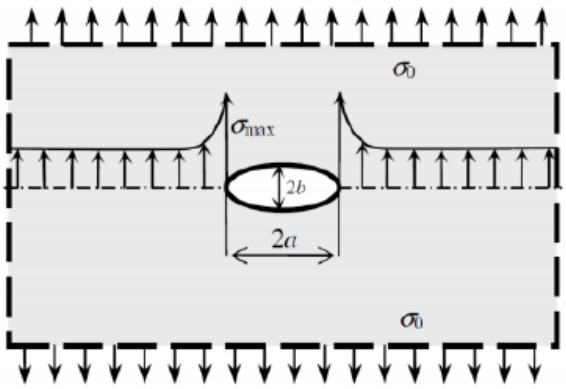

Figure 1.2 Elliptical hole in an infinite plate

1.2 Analytical Solution and FEM Analysis

Several FEM analyses were performed on a perforated plate, both in aluminum alloy and in composite material, to compare both the numerical results with the analytical ones and to compare the stress concentration factor values for both types of plates. Plates with circular holes of different sizes were examined.

1.2.1 Aluminum Alloy

The following tables report the geometric data of the two modeled plates, the load, and the data related to the material used. Two identical plates differing only in the size of the hole were considered.

a	1 m
b	1 m
t	0.0036 m
R_1	0.05 m
R_2	0.005 m
F	1 N

Table 1.1 Dimensions and load

E	70 GPa
ν	0.33

Table 1.2 Aluminum characteristics

Figures 1.3-1.4 show the FEM model, with applied loads and constraints. The applied tensile load is unitary and uniformly distributed on one side. The mesh was refined in the area adjacent to the hole to obtain greater accuracy of the results.

The analysis results are reported below. Figures 1.5-1.6 show the stress contours for the entire plate and around the hole, where they are intensified.

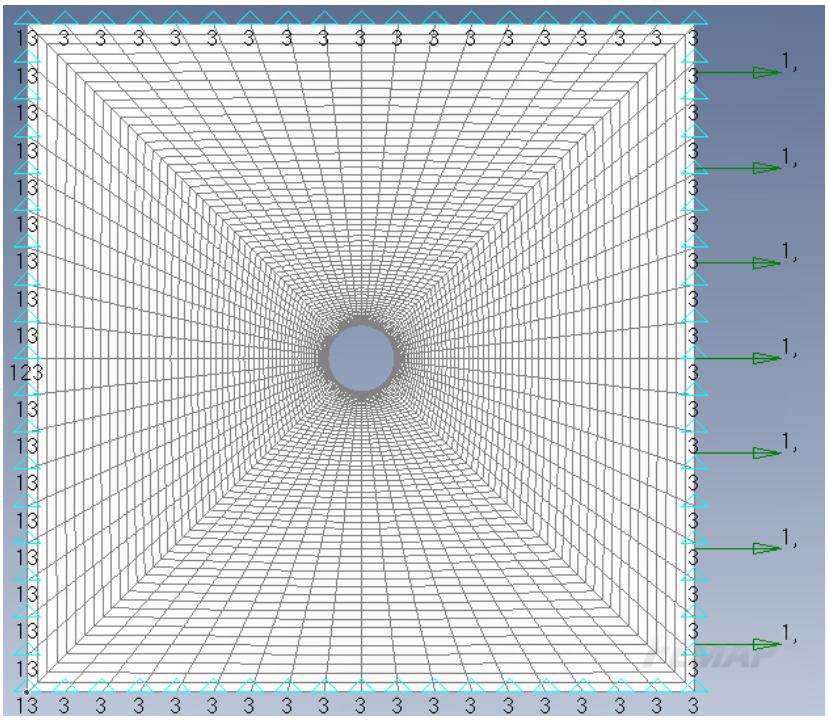

Figure 1.3 Mesh, load, and constraints on a plate with a hole of radius $R_1 = 0.05$ m

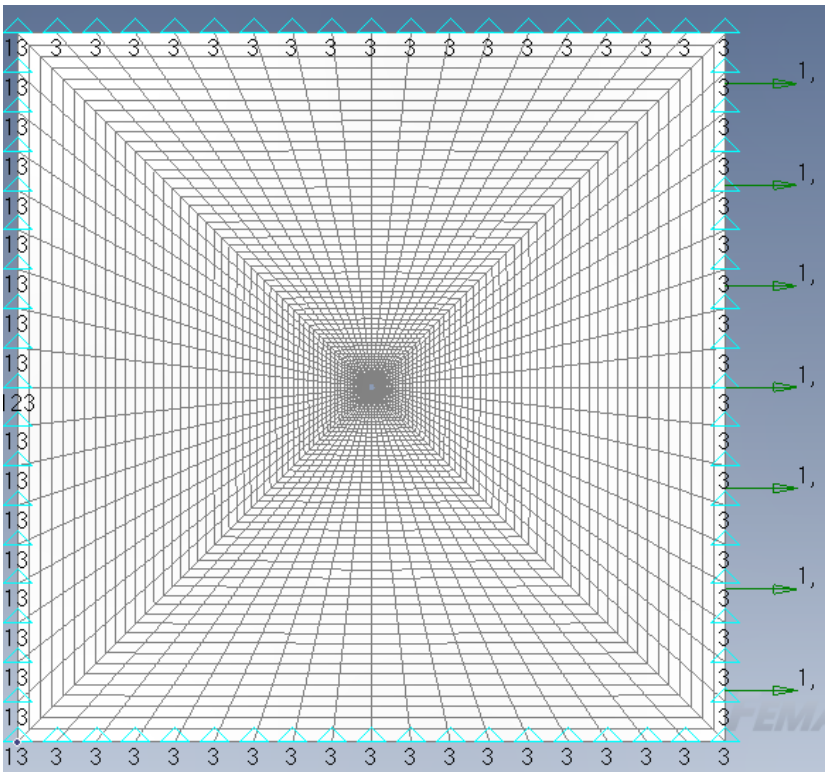

Figure 1.4 Mesh, load, and constraints on a plate with a hole of radius $R_2 = 0.005$ m

Figure 1.7 shows the trend of the stress concentration factor K_t, starting from the hole and moving towards the edge. It is particularly observed how the analytical solution becomes better as the size of the hole decreases relative to that of the plate. The numerical results, in terms of σ_0, σ_{max}, and K_t, are reported in Table 1.3, along with the percentage error. Only the results for the small hole are reported.

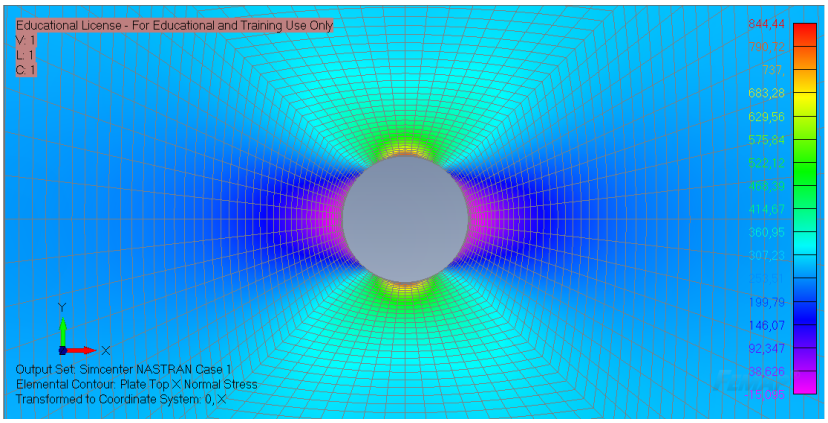

Figure 1.5 Contour of stress σ_x.

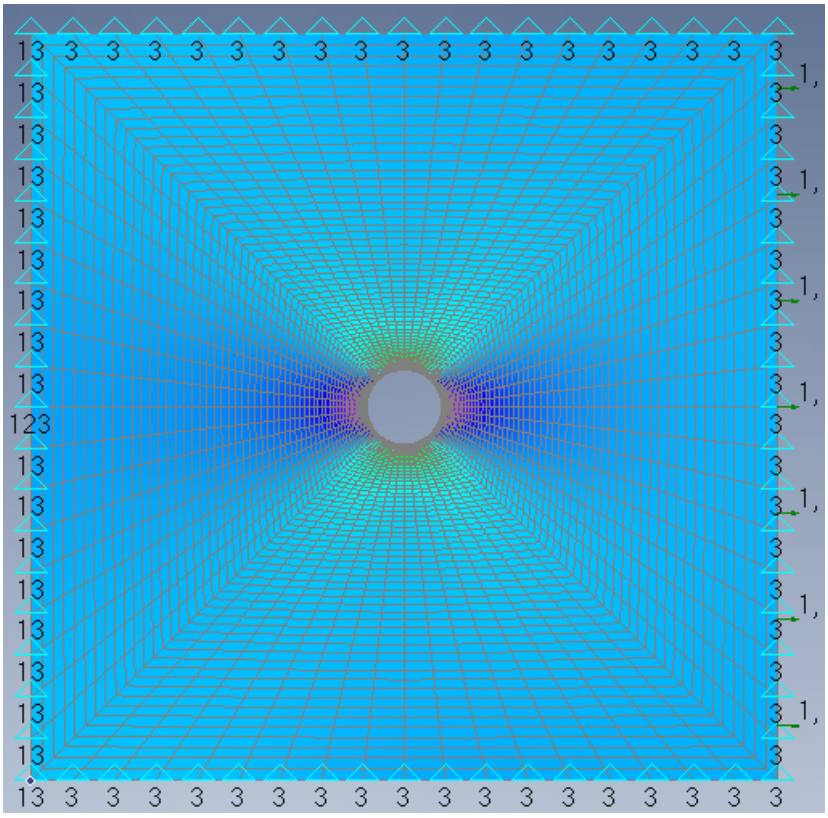

Figure 1.6 Contour of stress σ_x, detail around the hole.

Property	Value
σ_0	277.69 Pa
σ_{max}	824.72 Pa
$K_{t,\text{FEM}}$	2.97
$K_{t,\text{an}}$	3
Err (	

Table 1.3 Results for perforated aluminum plate

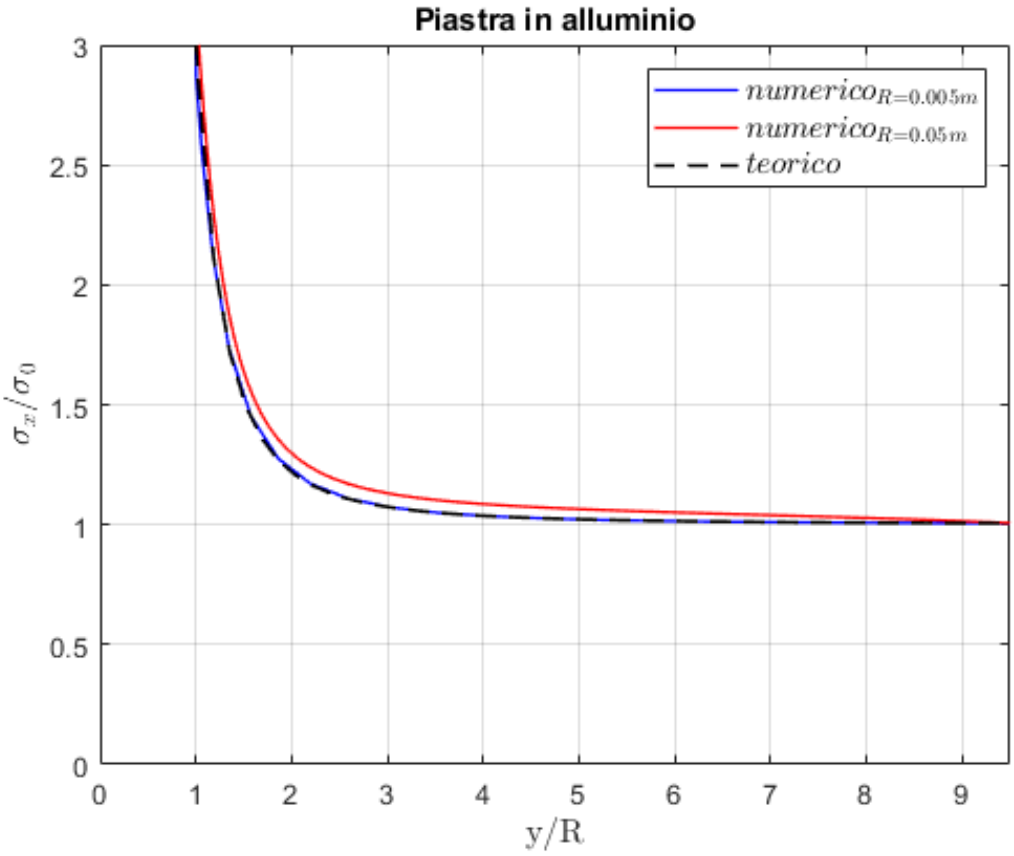

Figure 1.7 Trend of σ_x/σ_0 with distance y from the hole

1.3 Composite Material Ply

After analyzing the case of the aluminum alloy plate, various lamination sequences were analyzed for a composite plate of the same dimensions and thickness, to see how the stress concentration factor K_t varied according to the orientation angle of the plies, given a fixed total number of plies. Before analyzing the different laminates, the behavior of a single ply was analyzed by varying the fiber orientation with respect to the load direction. The ply orientation angles considered were: 0°, 30°, 45°, 60°, 90°. The composite material Graphite/Epoxy BMS 8-212 Type II Class 1, already seen in previous chapters, was considered, with properties shown in Table 1.4. Figures 1.8-1.12 show the stress contours around the hole for the different plies. Finally, Figure 1.13 reports the trend of stresses as a function of the angular position θ around the hole for the different plies. It is observed how significantly the position around the hole where the maximum stress occurs changes. While for plies at 0° and 90° the maximum stress is observed at $\theta = 90°$ due to the geometric, constraint, load, and material symmetry of the problem. For plies at 30°, 45°, 60°, symmetry is lost, and the maximum stress is obtained at different angular positions. It is also observed that not only the position of the maximum but also its value changes with the fiber orientation. The minimum stress occurs for plies oriented at 90°, while the maximum stress case is obtained for plies oriented at 0°. Based on these results, we can observe that generally, if the loading direction of the laminate is not known a priori, it is always convenient to use laminates with a high percentage of plies with different orientations, particularly at ±45°, to reduce the problem of stress intensification due to drilling. This result can be observed even more clearly with the laminate analysis

conducted in the next paragraph.

Property	Value
E_1	125 GPa
E_2	12.5 GPa
G_{12}	6.89 GPa
ν_{12}	0.38
ν_{21}	0.038
ρ	1400 kg/m^3

Table 1.4 Properties of Graphite/Epoxy

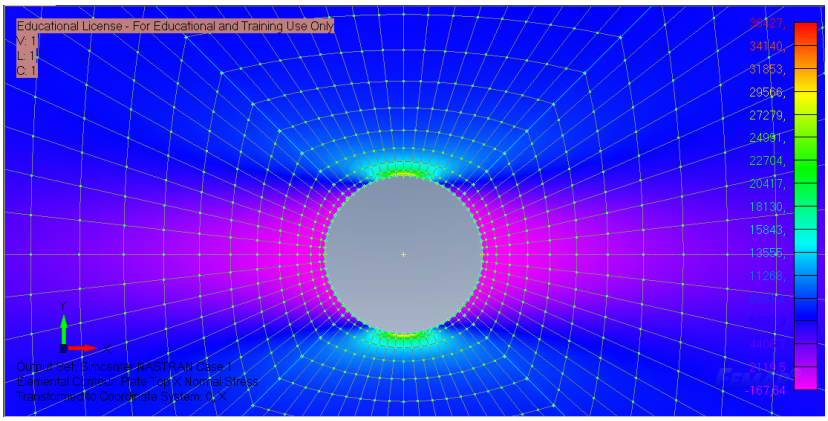

Figure 1.8 σ_x contour for a ply oriented at $\alpha = 0°$

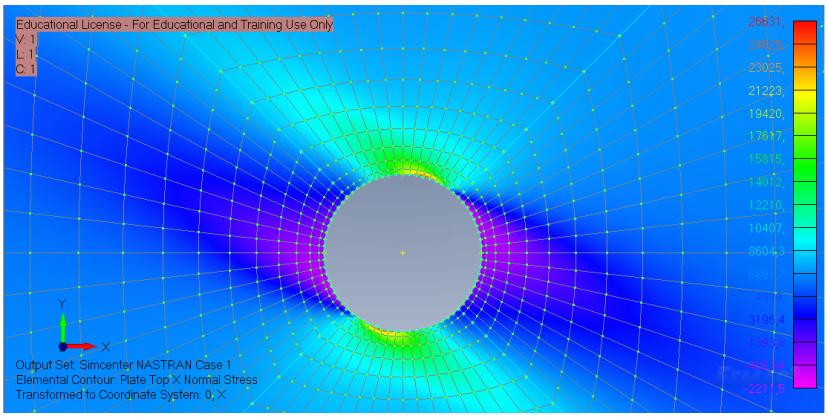

Figure 1.9 σ_x contour for a ply oriented at $\alpha = 30°$

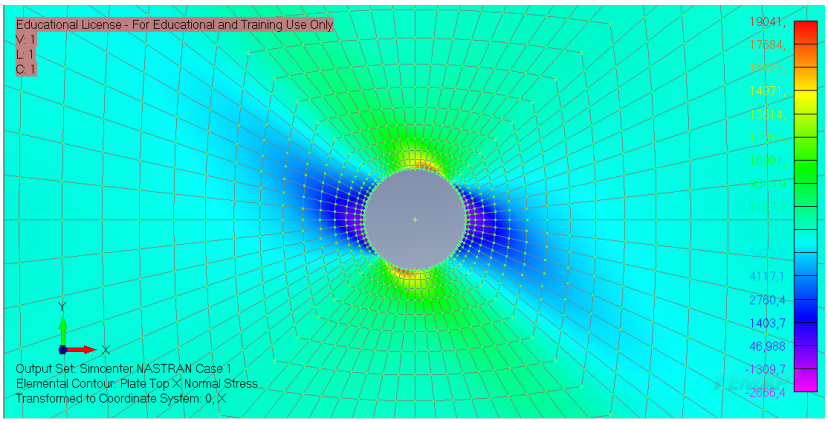

Figure 1.10 σ_x contour for a ply oriented at $\alpha = 45°$

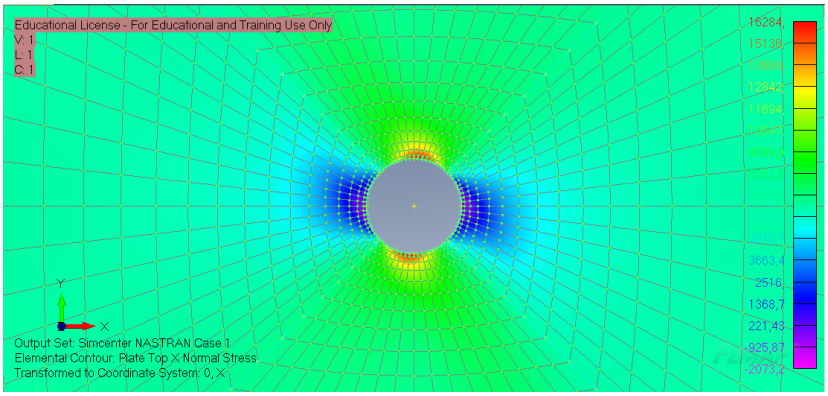

Figure 1.11 σ_x contour for a ply oriented at $\alpha = 60°$

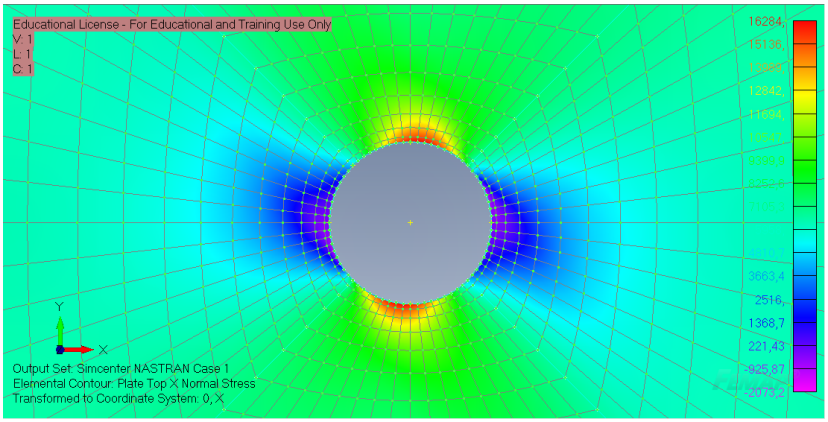

Figure 1.12 σ_x contour for a ply oriented at $\alpha = 90°$

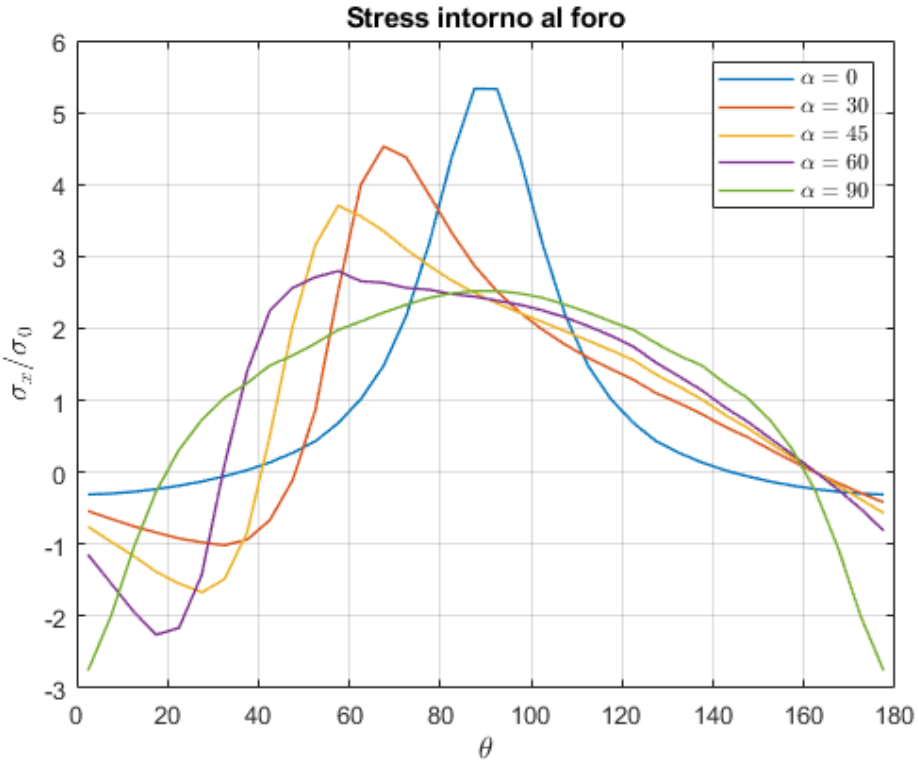

Figure 1.13 Trend of σ_x with varying angular position θ (deg)

1.4 Composite Material Laminate

Various lamination sequences were analyzed, and it is observed how the stress concentration factor K_t varies according to the orientation angle of the plies, given a fixed total number of plies. For each sequence, two identical plates differing only in the size of the hole were considered. The geometric data of the two modeled plates and the load are the same as those considered for the aluminum plate and reported in Table 1.1. The loads, constraints, and mesh are those of the FEM models previously shown in Figures 1.3-1.4 and used for the aluminum plate. In particular, the mesh was refined in the area adjacent to the hole to obtain greater accuracy of the results. The studied lamination sequences are:

- $[0°]_{24}$
- $[90°]_{24}$
- $[0°/90°]_{6s}$
- $[\pm 45°]_{6s}$
- $[0°/\pm 45°/90°]_{3s}$

For each sequence, the equivalent σ_x stress contour of the laminate around the hole and the trend of the stress concentration factor with varying distance y from the hole are shown for the two different hole radii.

1.4.1 Sequence $[0°]_{24}$

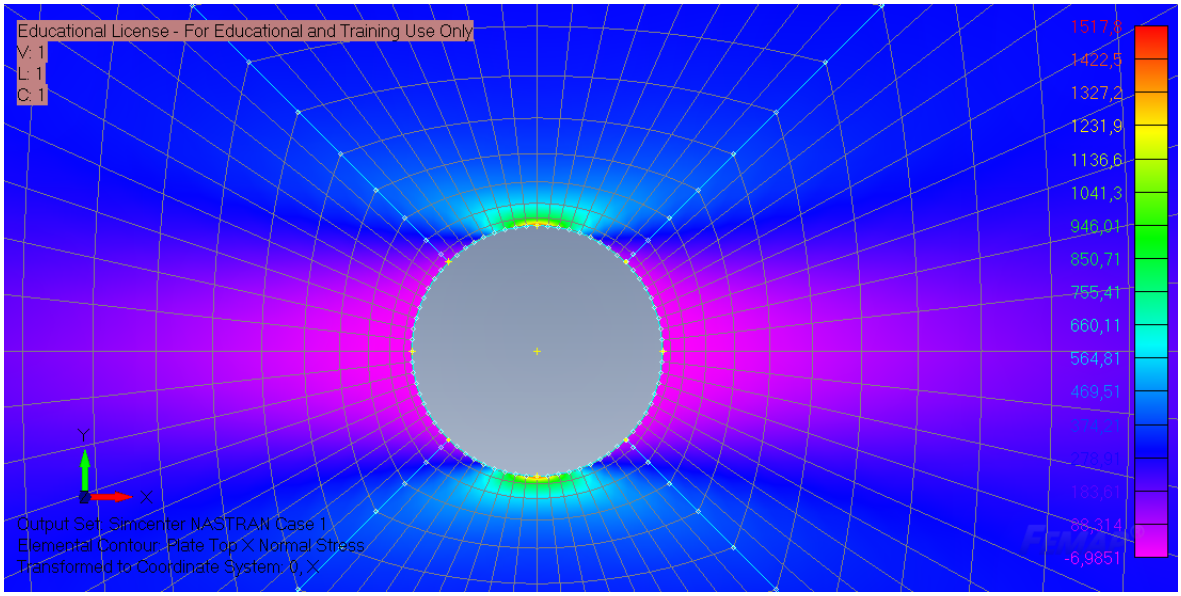

Figure 1.14 σ_x contour for the $[0°]_{24}$ sequence

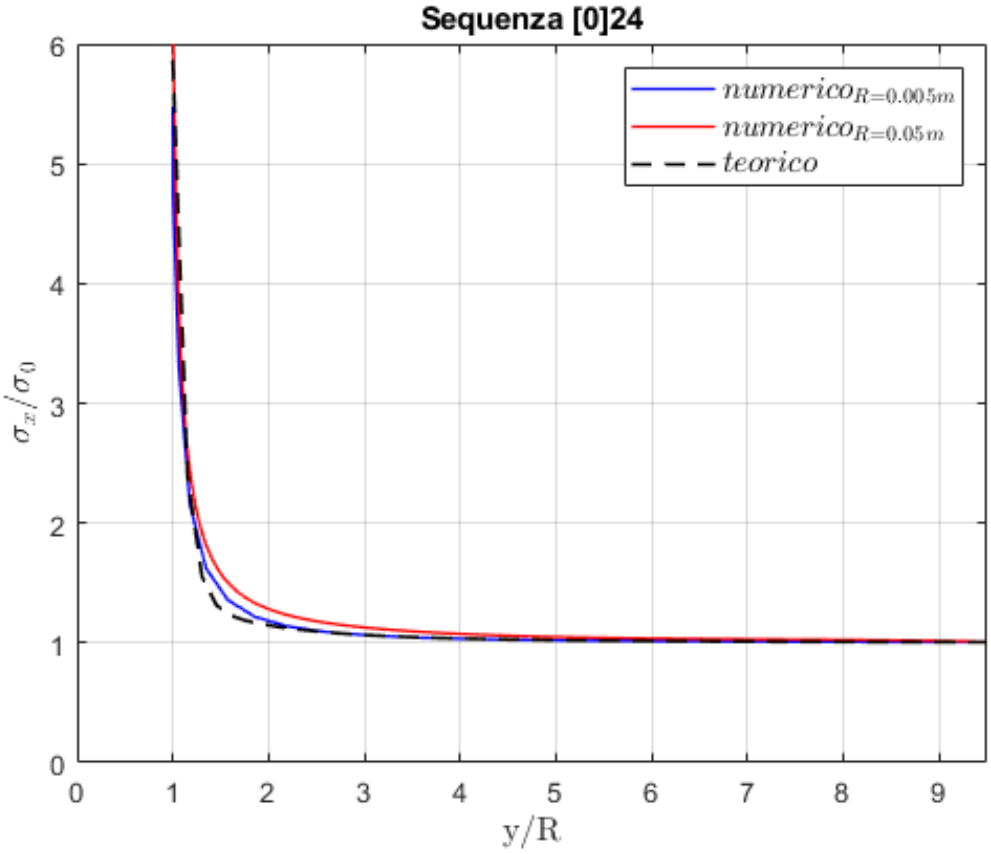

Figure 1.15 σ_x trend with varying distance y from the hole for the $[0°]_{24}$ sequence

1.4.2 Sequence $[90°]_{24}$

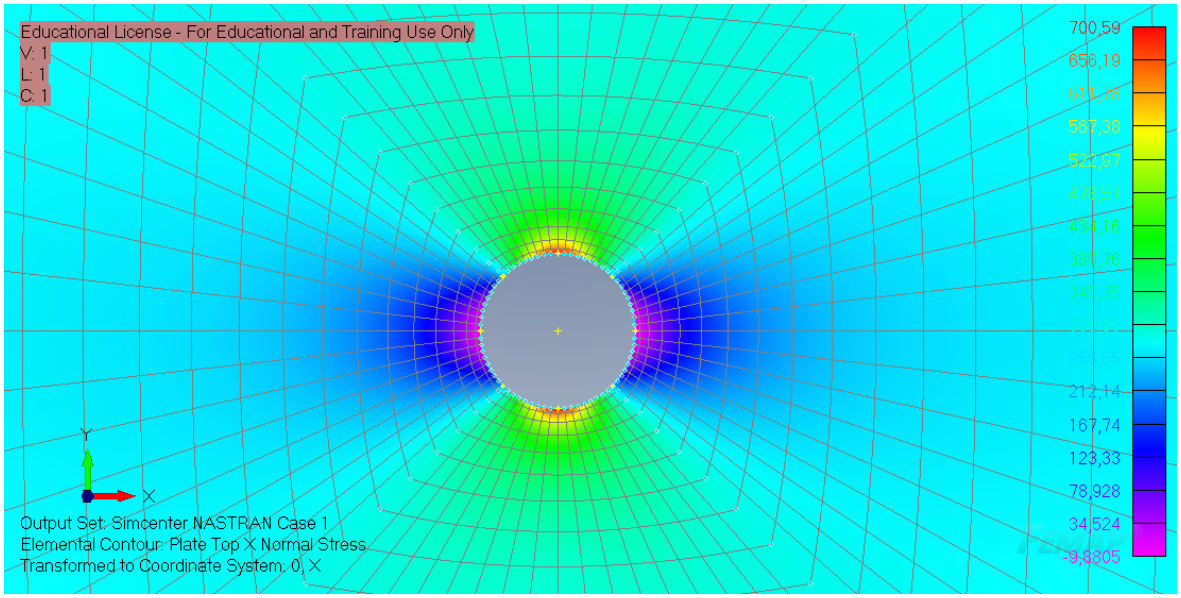

Figure 1.16 σ_x contour for the $[90°]_{24}$ sequence

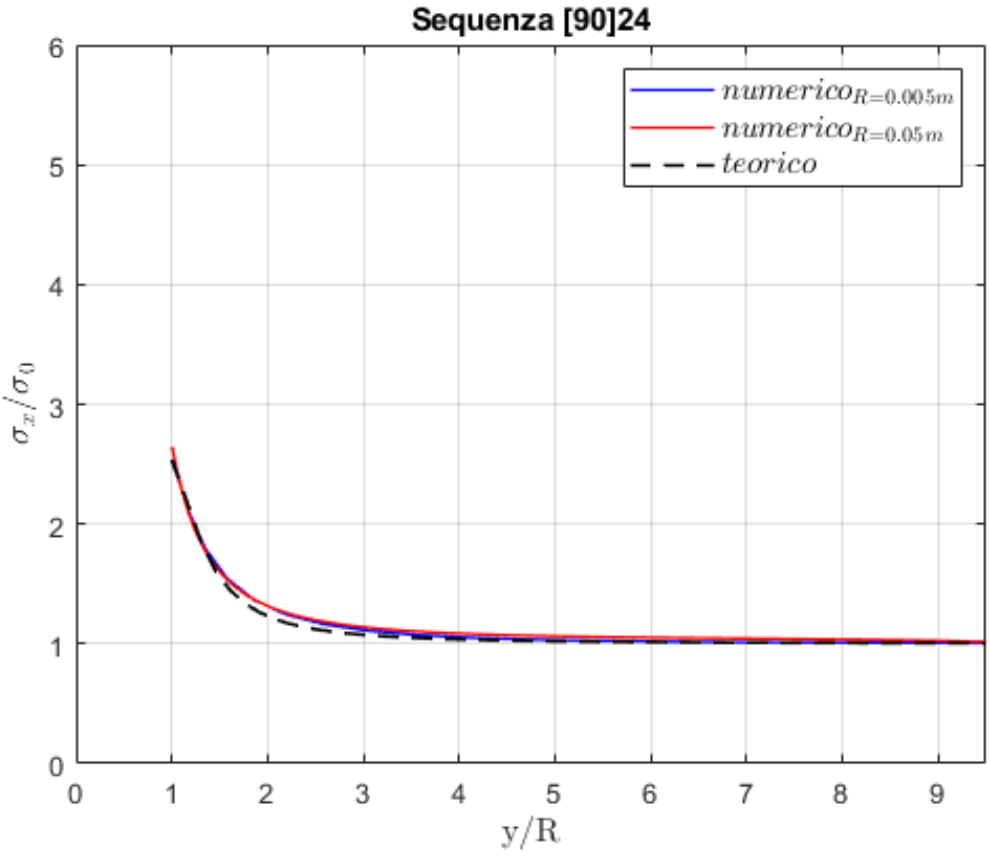

Figure 1.17 σ_x trend with varying distance y from the hole for the $[90°]_{24}$ sequence

1.4.3 Sequence $[0°/90°]_{6s}$

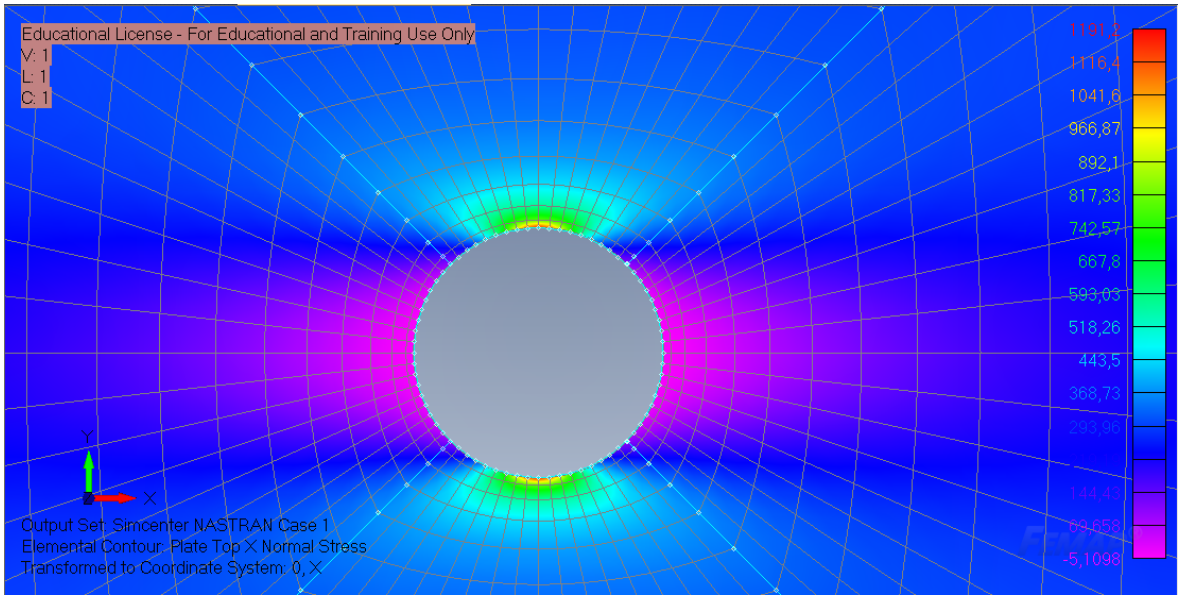

Figure 1.18 σ_x contour for the $[0°/90°]_{6s}$ sequence

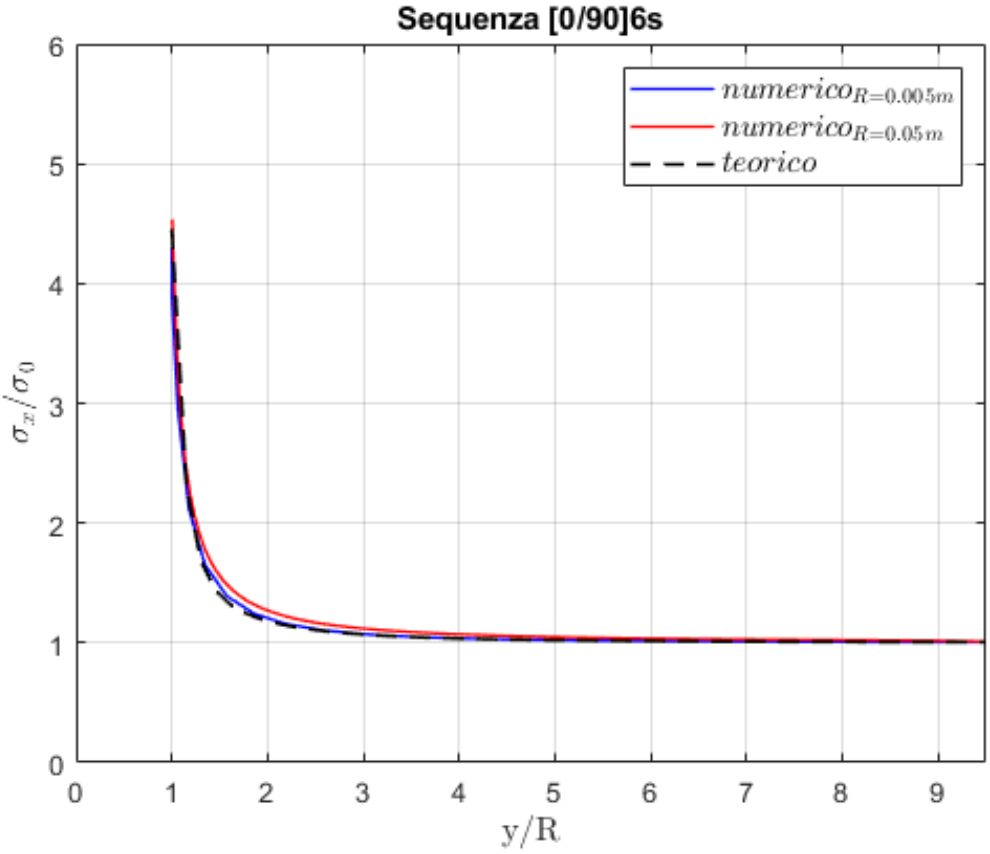

Figure 1.19 σ_x trend with varying distance y from the hole for the $[0°/90°]_{6s}$ sequence

1.4.4 Sequence $[\pm 45°]_{6s}$

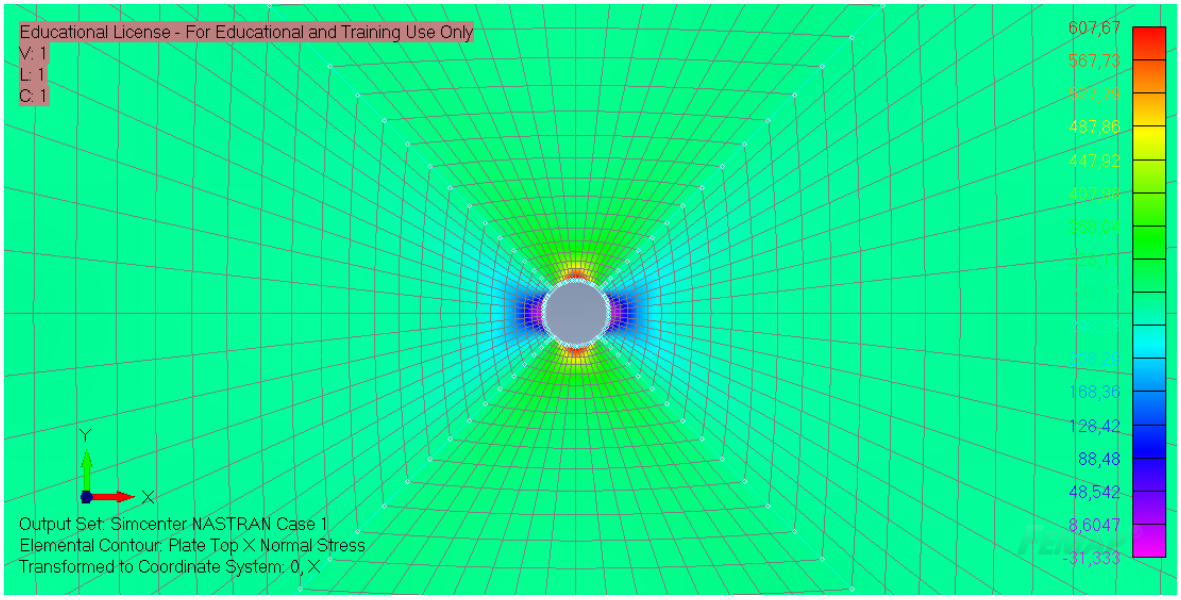

Figure 1.20 σ_x contour for the $[\pm 45°]_{6s}$ sequence

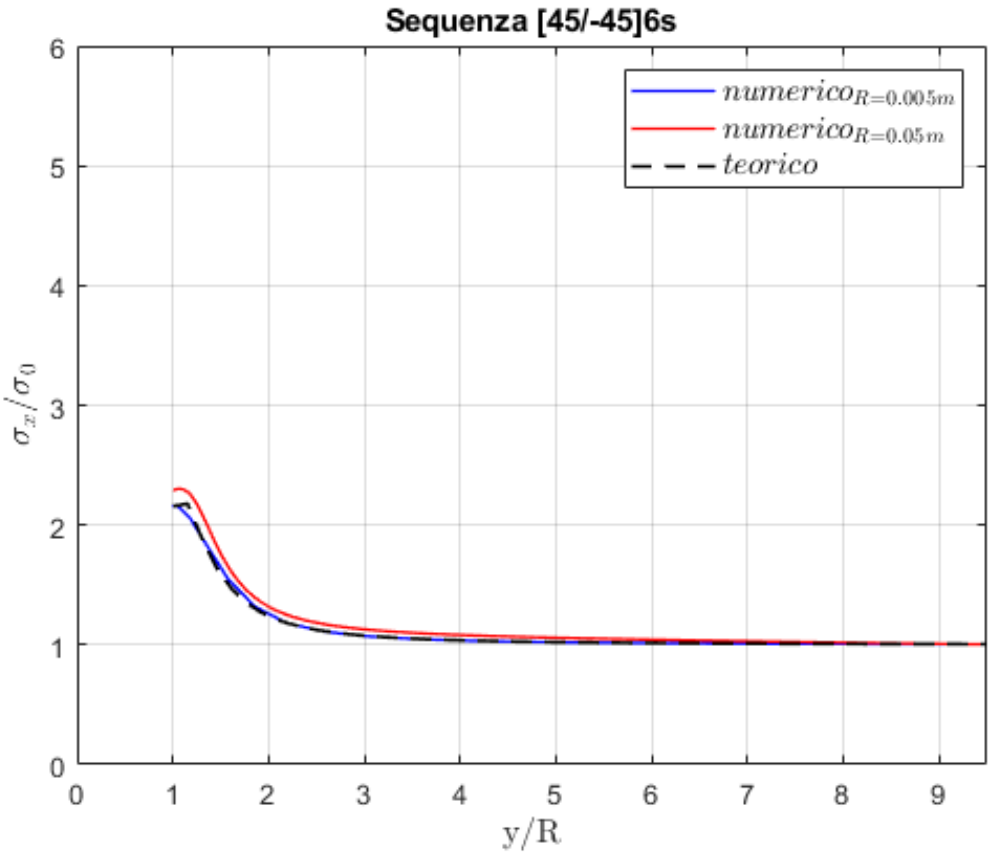

Figure 1.21 σ_x trend with varying distance y from the hole for the $[\pm 45°]_{6s}$ sequence

1.4.5 Sequence $[0°/\pm45°/90°]_{3s}$

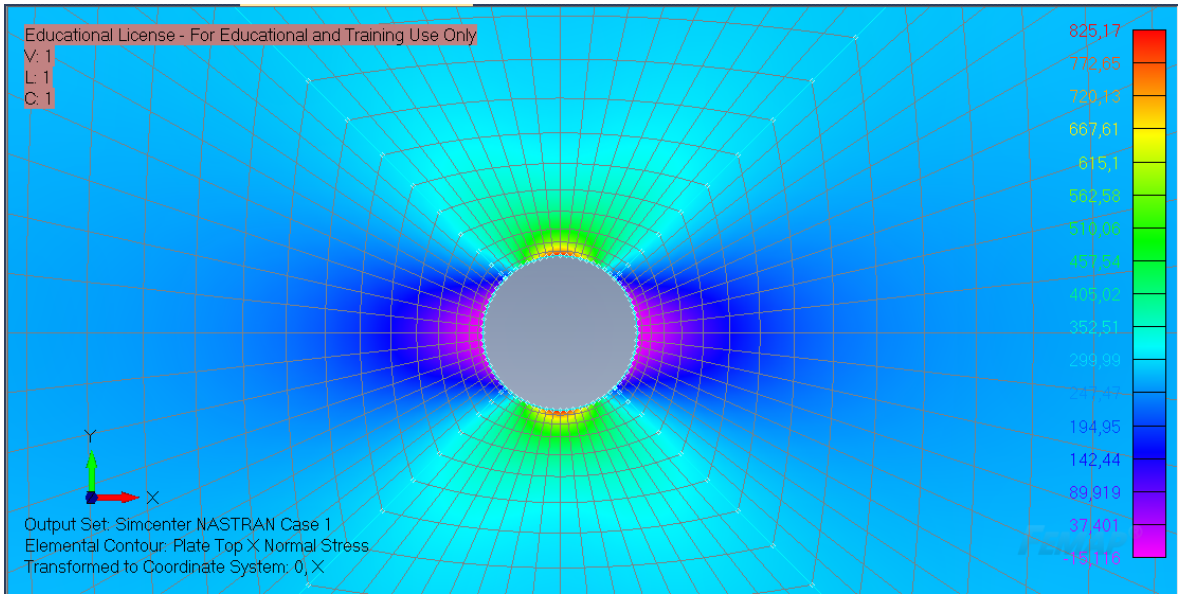

Figure 1.22 σ_x contour for the $[0°/\pm45°/90°]_{3s}$ sequence

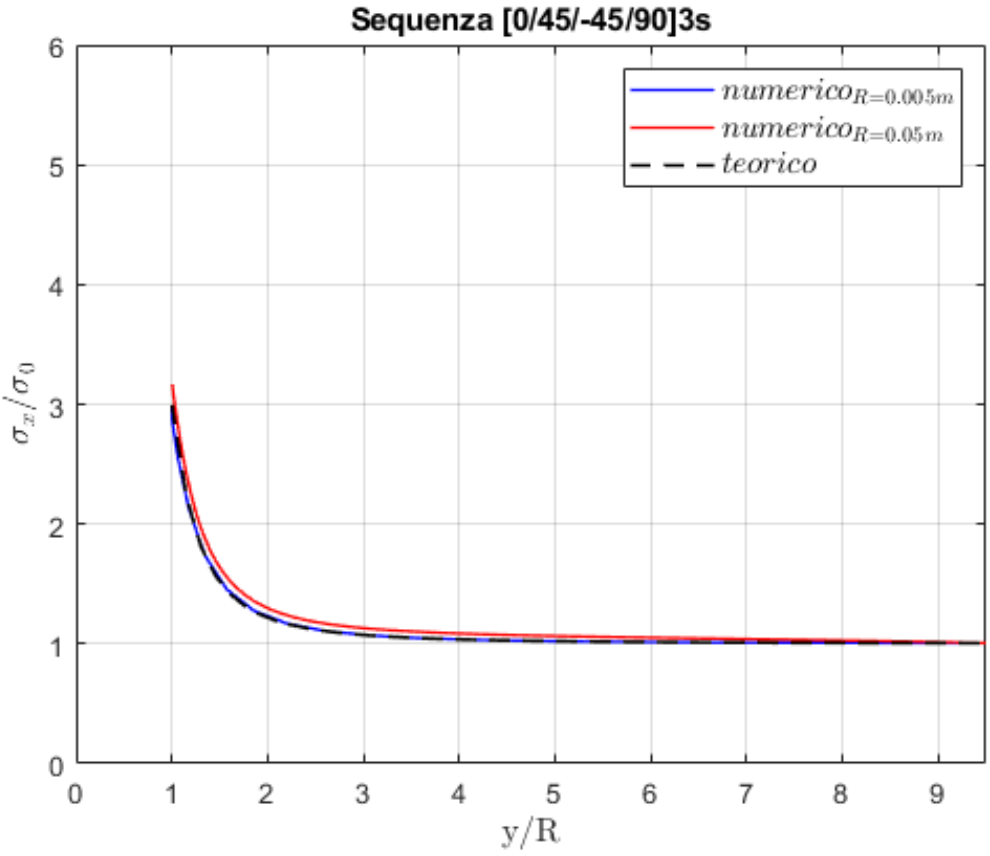

Figure 1.23 σ_x trend with varying distance y from the hole for the $[0°/\pm45°/90°]_{3s}$ sequence

1.4.6 Final Considerations

Figures 1.25-1.24 report the results for the different sequences in terms of the σ_x trend with varying distance y from the hole and the numerical results in terms of σ_0, σ_{max}, K_t, and percentage error. From the results, we can conclude that:

- the value σ_0 is always equal to that present in the laminate without a hole (277.69 Pa).
- The stress concentration factor K_t can vary greatly with the lamination sequence.
- For a laminate with all plies oriented at 0°, the stress value near the hole is almost 6 times higher than that without the hole. The increase occurs very sharply only in the vicinity of the hole. Due to the strong gradient near the hole, the numerical calculation is heavily influenced by the discretization, and it is necessary to greatly refine the mesh near it. Indeed, it is noted that the error is decidedly larger than that committed in evaluating K_t for the other sequences. Similar considerations also apply to the cross-ply $[0°/90°]_{6s}$.
- The minimum stress concentration factor occurs for a $[\pm 45°]_{6s}$ laminate. For this laminate, the increase also occurs very gradually, which is why the numerical estimation is extremely accurate. In general, it is observed that to reduce the problem of the high stress concentration factor that occurs around the hole, it is necessary to use high percentages of plies at ±45°.
- For quasi-isotropic laminates such as the $[0°/\pm 45°/90°]_{3s}$ laminate, the stress concentration factor tends to 3, as for isotropic materials.

Sequenza	σ0	σmax	Kt_teorico	Kt_numerico	Err(perc)
alluminio	277.69	824.72	3	2.97	1
[0]24	277.71	1521.14	5.87	5.48	6.67
[90]24	277.71	701.98	2.54	2.53	0.47
[0/90]6s	277.7	1193.6	4.46	4.3	3.52
[+-45]6s	277.7	600.54224	2.16	2.16	0.079
[0/+-45/90]3s	277.7	826.84	3	2.98	0.75

Figure 1.24 Numerical results for the different sequences, stresses are expressed in Pa

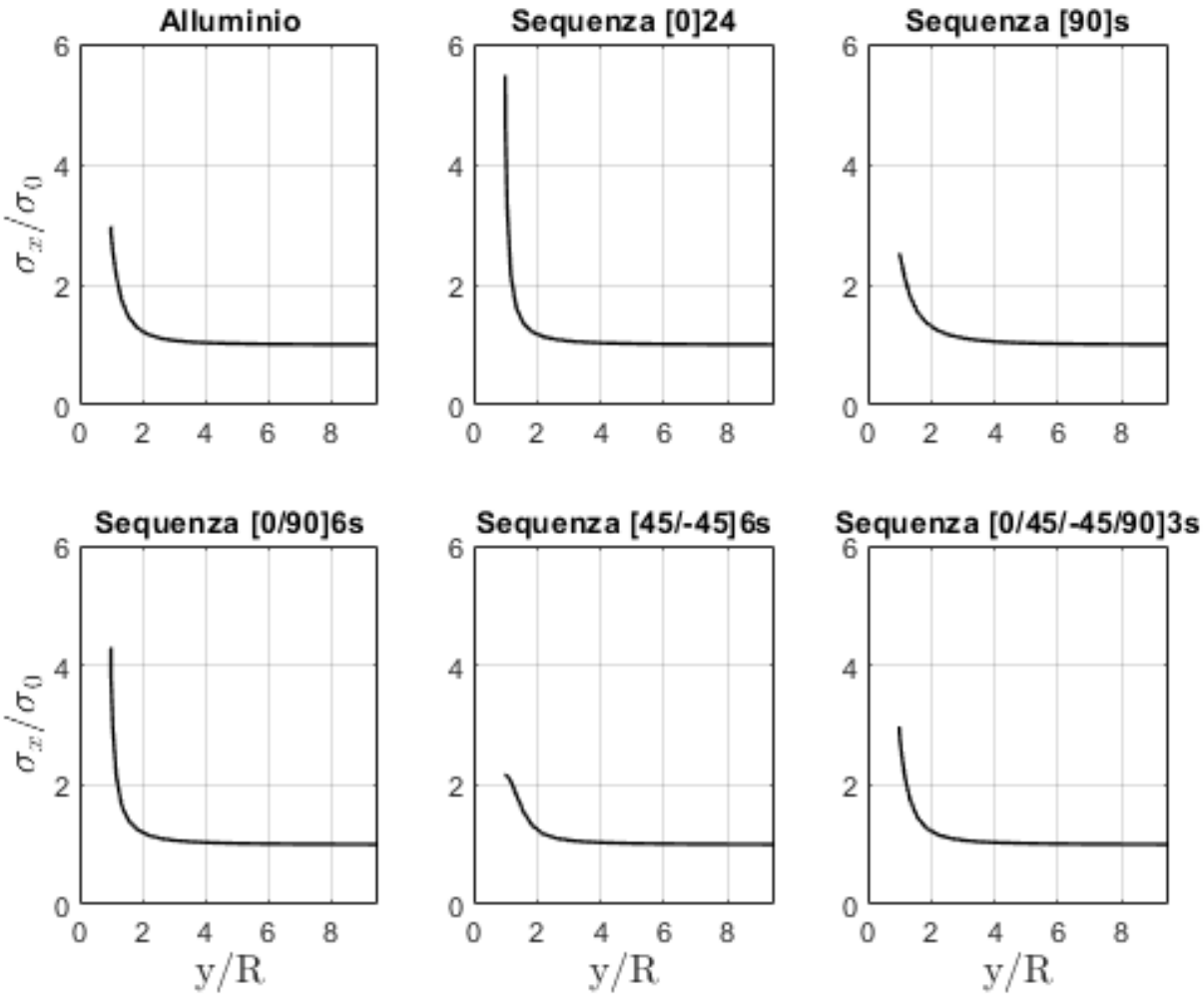

Figure 1.25 σ_x trend with varying distance y from the hole for the different sequences

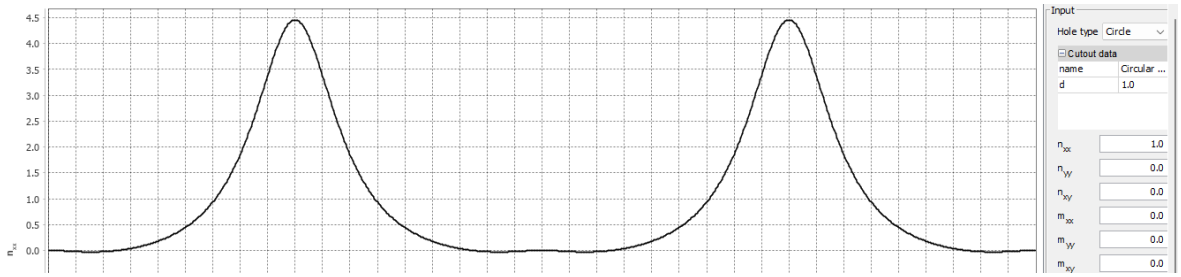

Figure 1.26 σ_x trend with varying distance y from the hole obtained for the $[0°/90°]_{6s}$ sequence with Elamx2 software. The results are almost identical to those theoretically predicted.

Chapter 2

Fracture Mechanics

2.1 Introduction to Fatigue and Fracture Mechanics

Fatigue is a phenomenon that occurs in materials when they are subjected to repeated cycles of loading and unloading. It is observed that even if the stress applied in each cycle is below the material's strength limit, the accumulation of stresses over time causes the formation of microcracks. These microcracks may already be present in the material's grains and are initially so small that they are not observable under a microscope. This first phase is called nucleation, and during this stage, propagation occurs very slowly. After this initial phase, the stable propagation phase begins, during which the crack is visible but still grows at a very low rate. In the final phase, growth occurs at a very high rate, leading to material failure. This phenomenon is particularly relevant in the aerospace field, where aircraft structures are continuously stressed during flight due to load cycles, such as pressure variations and aerodynamic forces.

The phenomenon was not first observed in the aerospace field, but as early as 1850, the German engineer Wöhler studied fatigue-related problems in railway carriages. He is credited with the S-N curves (or Wöhler curves) of materials, used in cumulative damage theory to estimate the number of cycles a component can withstand before failing.

The study of fatigue focuses on determining the number of cycles a component can withstand before failing and does not investigate what happens between the initiation of the crack and failure. Based on this discipline, the Safe Life maintenance criterion can be adopted, which involves replacing the component as soon as visible damage appears. However, this criterion is economically burdensome, as a component with visible damage might still be able to absorb loads without compromising safety. If one can determine how quickly the damage grows and when it becomes critical, the component can be used for its entire lifespan.

This is the idea behind the Damage Tolerance criterion, which is based on fracture mechanics, a discipline that studies and models crack propagation. Understanding fracture mechanics and fatigue is fundamental to ensuring the safety and reliability of aircraft. Advanced analysis and control approaches are essential to manage these phenomena and ensure the structural integrity of aerospace components.

2.2 Fracture Mechanics

2.2.1 Griffith's Criterion

In fracture mechanics, the crack is considered to be already present within the material, and its evolution until failure is studied. The crack is considered a discontinuity within the material. As already observed in the previous chapter, a discontinuity within a material always leads to an accumulation of stress around it. In particular, the stress concentration factor K_t was defined, and it was observed that in the vicinity of an elliptical hole in an infinite plate made of isotropic material (as in Fig.2.1), this quantity takes the form:

$$K_t = 1 + 2\frac{a}{b} \tag{2.1}$$

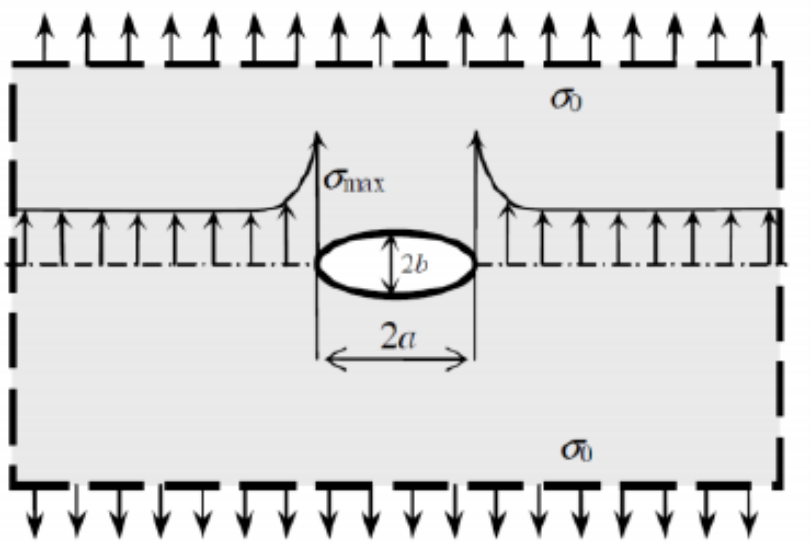

Figure 2.1 Elliptical hole in an infinite plate

A crack can be imagined as an elliptical hole for which the dimension b→0. Consequently, this static approach predicts that $K_t \rightarrow \infty$ around the crack, and therefore $\sigma_x \rightarrow \infty$ regardless of the applied asymptotic stress value. The static approach is then inadequate to describe the phenomenology because if the stress around the hole were to diverge for any load value, the crack should always propagate unstably, which is not what happens. In reality, the crack only propagates when the load is sufficiently high to exceed a critical value. The static approach fails because it is based on the assumption of linear elastic behavior of the material, an assumption that breaks down when considering that the stress around the crack becomes such that it causes the material to plasticize. Because this happens, the stiffness of the material decreases around the crack, and this means the material absorbs a lower stress value than predicted by the static approach; the remaining part is absorbed by the more distant material that continues to work in the linear elastic regime. Therefore, to study crack propagation, it is necessary to resort to an energy approach. In particular, for a plate with a crack on one side of initial size 'a' subjected to a constant load P (as shown in Fig.2.2), Griffith's criterion can be used to address the fracture problem. The material affected by crack propagation, before it occurs, has a certain state of strain and stress, thus storing a certain amount of elastic strain energy.

Following propagation, this energy is released. Griffith observed that an energy balance is established between the energy released during the fracture propagation process and the change in the internal energy of the plate. Specifically:

$$dW_s = dU \tag{2.2}$$

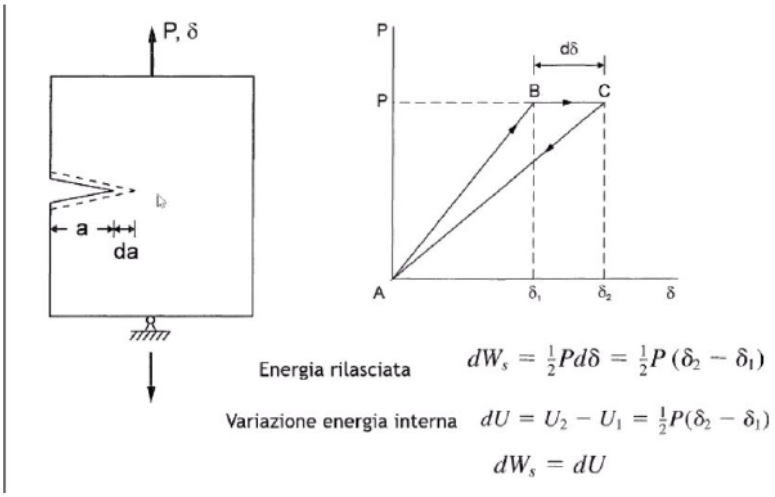

Figure 2.2 Crack in a plate.

Griffith's criterion states that if the released energy (W_s) reaches a value such that there is an equality between the energy required for propagation and the available energy, then propagation occurs. This criterion is formulated by defining the energy release rate:

$$G = \frac{dW_s}{t\,da} = \frac{dU}{t\,da} \tag{2.3}$$

Where t is the thickness of the ply, da is the length by which the crack increases, and consequently, their product represents the area of the surface liberated by the propagation. G thus represents the energy released per unit of liberated area. Griffith's criterion states that for propagation to occur, the energy release rate must be greater than or equal to a critical value:

$$G \geq G_{cr} \tag{2.4}$$

The factor G_{cr} is related to the fracture toughness of the material, denoted by K_{cr}, a quantity determined experimentally for each material and which changes depending on the crack mode that can occur (the three modes are shown in Fig.2.3). Fracture toughness also assumes different values depending on whether the plate is thick (and thus exhibits a plane strain state) or thin (and thus exhibits a plane stress state). Generally, however, only K_{cr} for a thick plate is tabulated, and that for a thin plate is obtained using the following relation:

$$\frac{K_{crit}}{K_{lc}} = 1 + B_k e^{-\left(A_k \frac{t}{t_0}\right)^2} \tag{2.5}$$

Griffith's criterion can be reformulated using the fracture toughness of the material as:

$$K_I \geq K_{cr} \tag{2.6}$$

Where K_I is called the Stress Intensity Factor (SIF) and can be evaluated as follows:

$$K = Y\sigma\sqrt{\pi a} \tag{2.7}$$

Where σ is the stress at a generic point in the plate. Y is the coefficient used to account for edge effects (it is unitary for a crack that is small compared to the plate dimensions). The SIF is an energy parameter and should not be confused with K_t, the stress concentration factor, which is a static parameter. It is shown that the SIF is related to the energy release rate by considering the energy involved in crack closure. Operationally, Griffith's criterion is used to determine, given the crack size (a), the load value that leads to its propagation. More often, it is used to determine the crack size at which it begins to propagate unstably due to a known applied load.

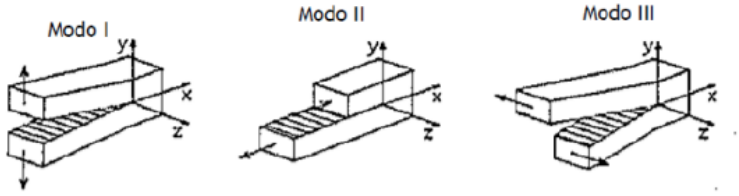

Figure 2.3 Opening mode (I), in-plane shear (sliding) mode (II), out-of-plane shear (tearing) mode (III)

2.2.2 Crack Propagation Models: Paris' Law

So far, it has been assumed that the external stress applied to the element with a crack was constant. However, the scenario where the external stress varies is more significant. This is because during fatigue cycling, crack propagation can occur even for stress values much lower than those associated with static fracture. This continuous propagation is due to variations in the accumulated elastic strain energy in the plate. For this reason, several models have been developed that link the crack propagation rate $\frac{da}{dN}$ to

$$\Delta K = Y\Delta\sigma\sqrt{\pi a} \tag{2.8}$$

i.e., the range of variation of the stress intensity factor, which, as already observed, is an energy parameter. One of the simplest models developed is Paris' Law:

$$\frac{da}{dN} = C(\Delta K)^m \tag{2.9}$$

In it, the coefficients C and m are treated as constants that depend only on the material. A more adequate model should account for the variation of these parameters with the crack size itself. Figure 2.4 shows the typical trend of the crack propagation rate on a log-log scale. From the figure, three phases of propagation can be observed:

- An initial nucleation phase where the crack is very small, and the propagation rate is small but increases rapidly.
- The second phase is stable growth, and the trend is linear on the log-log scale.

- In the final phase, the rate increases very rapidly, and fatigue failure occurs.

It is also observed from the graph that Paris' Law only correctly predicts the trend in the second, stable growth phase. The law is too approximate for the other phases. The reason it is often used is that it is very simple to integrate and thus allows:

- either to determine how the crack size 'a' varies with the number of cycles N, given the initial size a_0.

$$a = \left[\left(-\frac{m}{2}+1\right) C(\sigma_0^2\pi)^{m/2} N + a_0^{-m/2+1}\right]^{1/(-m/2+1)} \tag{2.10}$$

- or to determine the final size, given the initial size and the number of cycles the load is subjected to.

- or to determine how many cycles are necessary to go from a fixed initial size to a fixed final size.

$$N = \frac{a^{1-m/2} - a_0^{1-m/2}}{1-m/2} \cdot \frac{1}{C(\sigma_0^2\pi)^{m/2}} \tag{2.11}$$

Besides Paris' model, more complex propagation models exist that also account for other parameters such as the stress ratio

$$R = \frac{\sigma_{max}}{\sigma_{min}} \tag{2.12}$$

The most general model, which is also implemented in software like AFGROW, is the NASGROW equation (Fig.2.5).

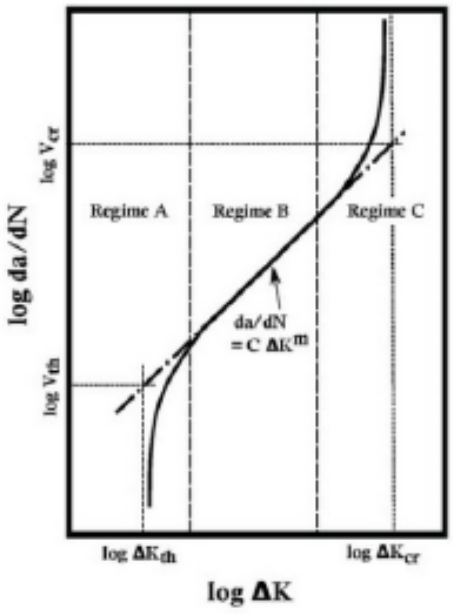

Figure 2.4 Comparison between Paris' Law and the typical trend of crack propagation rate

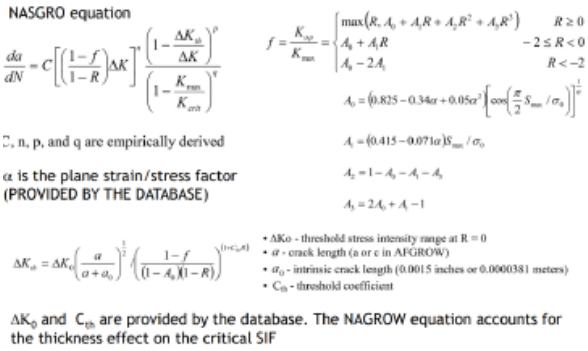

Figure 2.5 NASGROW model

2.3 Applications of Fracture Mechanics

In this section, applications of the principles underlying Linear Elastic Fracture Mechanics (LEFM) are proposed. The following exercises will consider a panel with a crack subjected to tensile loading as in Fig.2.6 with the following dimensions:

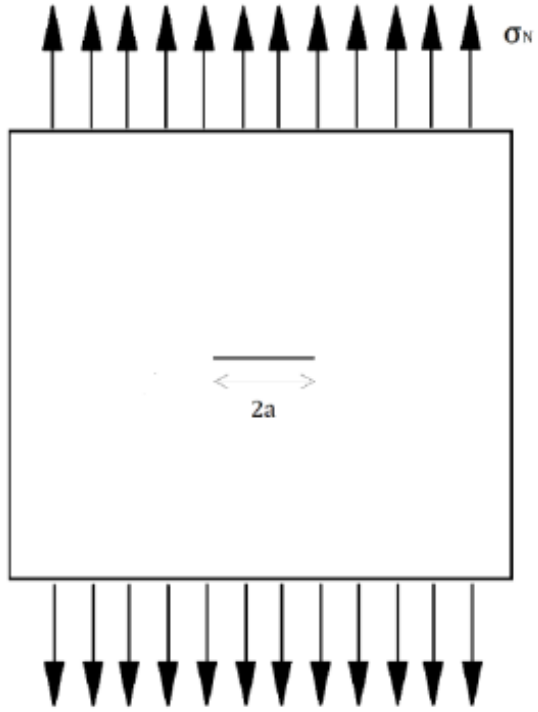

Figure 2.6 Plate with a crack

w	1 m
t	0.002 m
a	0.003 m

Table 2.1 Initial crack width, thickness, and size

2.3.1 Propagation Rate da/dN

As a first application, a code is proposed that allows studying the trend of the crack propagation rate in the panel with the assigned geometry using 3 different models: Paris' model, Walker's model, and NASGROW model. The material considered is aluminum alloy 2024-T3 Al with properties shown in Fig.2.7. A sinusoidal load spectrum with characteristics in Tab. 2.2 was considered. The results produced with the MATLAB script are also compared with those obtained with AFGROW software and shown in Fig.2.8. It is observed that the results produced in MATLAB are adequate only for high ΔK values. It is observed that Paris' and Walker's models are more conservative because they predict a higher propagation rate, but they are also less reliable. In particular, we observe that the trends predicted by Paris' Law and Walker's Law are different because R is different from 0.

σ_{max}	80 MPa
R	-0.1

Table 2.2 Load characteristics

Property	Value	Property Description
E	73084.4	Young's Modulus
Nu	0.33	Poisson's Ratio
AlphaT	2.32e-005	Coefficient of thermal expansion
UTS	66	Ultimate tensile strength
YS	365.422	Yield stress
K1e	50.547	Effective fracture toughness for surface/elliptica...
K1c	36.262	Plane strain fracture toughness
Ak	1	Fit Parameter
Bk	1	Fit Parameter
Rlo	-0.3	Negative cut-off stress ratio
Rhi	0.7	Positive cut-off stress ratio
C	1.5451e-...	Paris crack growth rate constant
n	3.284	Paris exponent in Forman-Newman-de Koning-H...
p	0.5	Exponent in Forman-Newman-de Koning-Henrik...
q	1	Exponent in Forman-Newman-de Koning-Henrik...
DKo	3.187	Threshold stress intensity factor range at R = 0
Cth	1.5	Threshold coefficient
Alpha	1.5	Plane stress/strain constraint factor
Smax/SIGo	0.3	Ratio of the maximum applied stress to the flow ...

Figure 2.7 Properties of 2024-T3 Al alloy

Listing 2.1

```
clc;
clear;
close all;

% Constants and parameters
K_crit = 72.524;
A_k = 1;
B_k = 1;
C = 1.545e-10;
n = 3.284;
p = 0.5;
q = 1;
delta_K_0 = 3.187;
C_th = 1.5;
alpha = 72.524/36.262;
```

```
S_max_sigma_0 = 0.1;
a = 0.003;
a_0 = 0.0000;
R = -0.1;
K_max = linspace(7, K_crit-0.1);

% Calculating constants A_0, A_1, A_2, A_3
A_0 = (0.825 - 0.34*alpha + 0.05*alpha^2) * (cos(pi/2 * S_max_sigma_0))
    ^(1/alpha);
A_1 = (0.415 - 0.071*alpha) * S_max_sigma_0;
A_3 = 2 * A_0 + A_1 - 1;
A_2 = 1 - A_0 - A_1 - A_3;

% Parameter lambda
lambda = 0.5;

% Conditional function for f based on R
if R >= 0
    f = max(R, A_0 + A_1*R + A_2*R^2 + A_3*R^3);
elseif -2 <= R && R < 0
    f = A_0 + A_1*R;
else
    f = A_0 - 2*A_1;
end

% Calculating delta_K_th
delta_K_th = delta_K_0 * sqrt(a/(a + a_0)) / (1 - f / ((1 - A_0) * (1 - R
    )))^(1 + C_th * R);

% Defining the delta_K range
delta_K = linspace(delta_K_th + 0.001, K_crit - 0.001);

% NASGRO equation
da_dN_nasgro = C * (((1 - f) / (1 - R)) * delta_K).^n .* (1 - delta_K_th
    ./ delta_K).^p ./ (1 - K_max / K_crit).^q;

dadN_Walker = [
    2   1.50491e-009
72.286  0.000196817
    ];

dadN_nas =[
3.08292 2.35577e-011
3.10368 1.11998e-010
3.13136 1.73113e-010
3.22132 3.14945e-010
3.42892 5.93046e-010
3.77493 1.10081e-009
4.46695 2.51187e-009
5.15896 4.64074e-009
6.54299 1.1854e-008
10.0031 5.76873e-008
16.9232 3.96695e-007
23.8434 1.44206e-006
30.7635 3.94908e-006
37.6837 9.32067e-006
```

```
44.6038 2.04073e-005
51.524  4.3911e-005
58.4441 0.000100005
65.3643 0.000289666
68.8244 0.000687023
71.7308 0.00491584
72.0768 0.0132792
72.2153 0.0397105
72.2222 0.044067
72.2775 0.352985
72.2845 2.79658
];



% Plotting NASGRO equation
figure(13);
loglog(delta_K, da_dN_nasgro, 'ob-');
axis([1 100 10^(-10) 10]);
xlabel('\DeltaK [Mpa*sqrt(m)]');
ylabel('da/dN [m/cycle]');
title('Confronto equazioni');
grid on;
hold on;
% Plotting NASGRO equation con AFGROW
loglog(dadN_nas(:,1), dadN_nas(:,2),'k-');

% Walker equation
da_dN_walker = C * delta_K.^n / (1 - R)^(n * (1 - lambda));
loglog(delta_K, da_dN_walker, 'or-');
% Walker equation con AFGROW
loglog(dadN_Walker(:,1), dadN_Walker(:,2),'k--','LineWidth',2);


% Paris equation
da_dN_paris = C * delta_K.^n;
loglog(delta_K, da_dN_paris, 'oy-');

% Legend and saving the figure
legend('NASGRO','NASGROWAFF', 'Walker','WalkerAFF', 'Paris');
hold off;
```

2.3.2 Variation of Crack Size with Number of Cycles

As a second application, a MATLAB program was written that allows integrating Paris' Law. The same geometry, material, and load spectrum as the previous exercise were considered. In particular, the code allows evaluating the K_{cr} for a thin plate from the tabulated value for a thick plate by implementing Eq.2.5. After that, the value of the static load that causes the crack to propagate is evaluated. Given the tensile load, the crack size from which it propagates is evaluated. In particular, it is first evaluated without considering the Correction Factor, then using an iterative method to account for the correction factor. Finally, Paris' Law is integrated numerically. The results are shown comparing them with those obtained with AFGROW. It is particularly observed that in

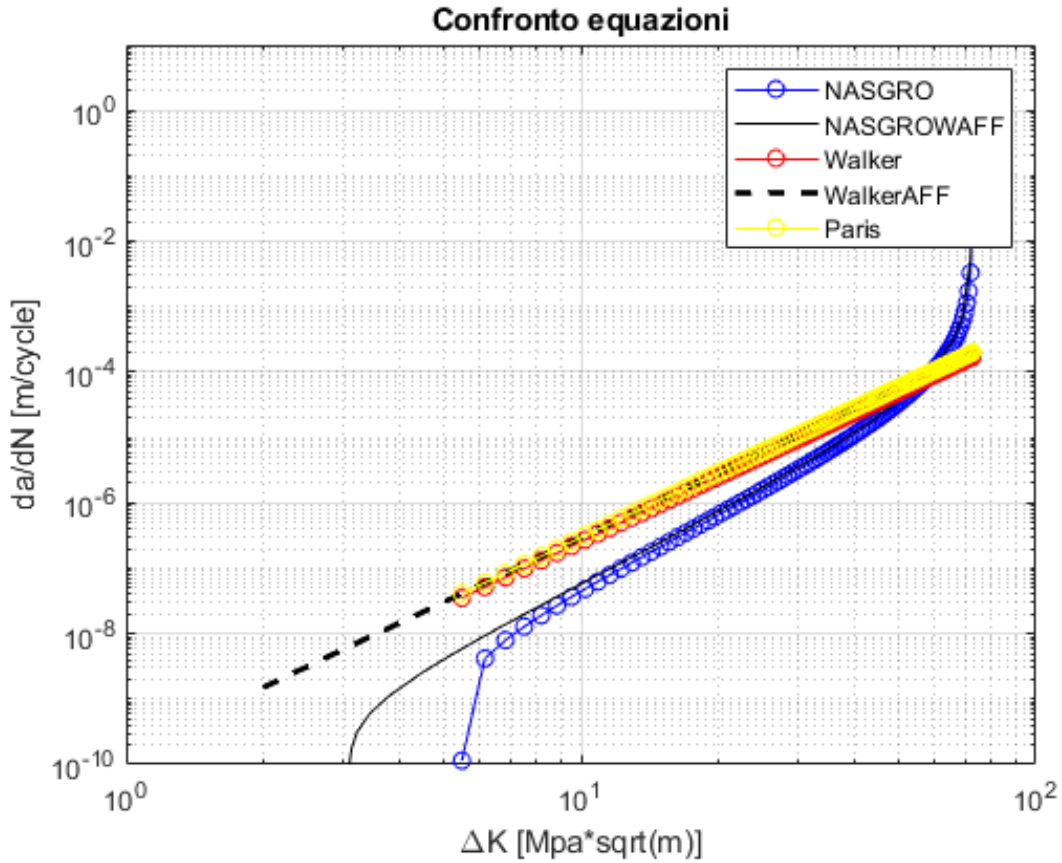

Figure 2.8 Comparison of propagation rate trends for different models, and between results produced in MATLAB and AFGROW

Paris' Law, the Beta correction factor should only be used to evaluate the crack size value that leads to plate failure, but it should not be used in the integration.

```
Il carico statico che porta alla propagazione della cricca è: 744.0235MPa
Senza tener conto del Correction Factor Y
La dimensione della cricca a partire dalla quale c'è propagazione: 0.25988m
Valore del fattore correttivo: 1.2029
Considerando il Correction Factor Y
La dimensione della cricca a partire dalla quale c'è propagazione: 0.20913m
Valore del fattore correttivo: 1.1147
>>
```

Figure 2.9 Results with and without Beta correction factor

Casi	Acr	Ncr	Y
AFFGROW	0.2104	33700	1.138
MatlabNocorr	0.2599	34014	1.2029
Matlabcorr	0.2091	18378	1.1147

Figure 2.10 Comparison of Y, a_{cr}, N values for the 3 cases

Listing 2.2

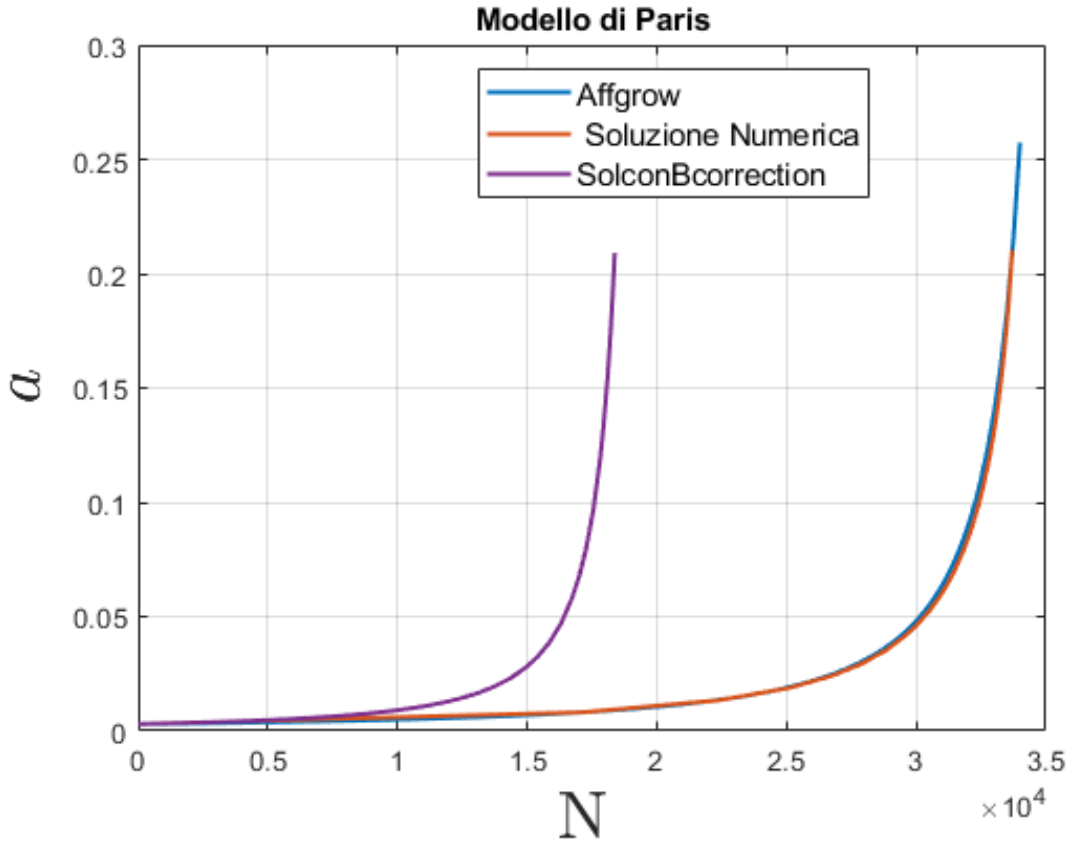

Figure 2.11 Trend of crack size with the number of cycles

```
clc;
clear;
close all;

%% Materiale Al 2024T3
sigma_y = 365.4; % Mpa
E = 73.084e3; % Mpa
nu = 0.33;
G = E/(1 -2* nu); %Mpa
K_1c_ = 36.262; % Mpa*m^0.5
Ak = 1;   % coef corr spessore
Bk = 1;   % coef corr spessore
% PARAMETRI MODELLO DI WALKER
m = 3.284;
C = 1.545e-10;

%% Geometria del pannello e della cricca
W = 1; %m
t = 0.002; %m

% tenacit  modificata per lo spessore
t_01 = 2.500 * (K_1c_/sigma_y)^2; %m

K_1c = K_1c_ * ( 1+Bk* exp(-Ak*(t/t_01)^2));

%% Esercizio 1 assegnato il valore della dimensione iniziale della cricca
%% valuto la tenzione critica che fa propagare la cricca
```

```
a_in = 0.003; %m
Yi = 1 + 0.256*(a_in /W) - 1.152 * (a_in/W)^2 + 12.2*(a_in/W)^3;
sigma_1cr = K_1c/(Yi*((pi*a_in)^0.5));

disp(['Il carico statico che porta alla propagazione della cricca   : ', num2str(sigma_1cr),'MPa'])
%disp(['Poich     pi   grande del carico di snervamento, la cricca non propaga staticamente'])
%% Esercizio 2 assegnato il valore della tenzione massima
%% valuto la dimensione della cricca a cui inzia la propagazione instabile
sigma_max = 80;
a_cr = (1/pi)*(K_1c/(sigma_max))^2;
disp(['Senza tener conto del Correction Factor Y'])
disp(['La dimensione della cricca a partire dalla quale c'' propagazione: ',num2str(a_cr),'m'])
Y_f_errato = 1 + 0.256*(a_cr /W) - 1.152 * (a_cr/W)^2 + 12.2*(a_cr/W)^3;
disp(['Valore del fattore correttivo: ',num2str(Y_f_errato)])
%% Metodo iterativo per trovare Y
err = 2;
tol = 1e-6;
i = 1;
Y_f_cor = 1;

while err > tol
a_cr_cor = (1/pi)*(K_1c/(Y_f_cor*sigma_max))^2;
Y_f_new = 1 + 0.256*(a_cr_cor /W) - 1.152 * (a_cr_cor/W)^2 + 12.2*(a_cr_cor/W)^3;
Y_f_cor = (Y_f_new + Y_f_cor)/2;
err =abs(Y_f_cor - Y_f_new);
i = i+1;
end

trova_a = @(a) K_1c - (sigma_max * ...
    (1 + 0.256*(a_cr_cor /W) - 1.152 * (a_cr_cor/W)^2 + 12.2*(a_cr_cor/W)^3) *...
    ((pi*a)^0.5));
a_tent = fzero(trova_a,0.19);
disp(['Considerando il Correction Factor Y'])
disp(['La dimensione della cricca a partire dalla quale c'' propagazione: ',num2str(a_cr_cor),'m'])
disp(['Valore del fattore correttivo: ',num2str(Y_f_cor)])
%% Esercizio 3 assegnato il valore della tenzione massima
%% valutata la dimensione della cricca a cui inzia la propagazione instabile
%% calcolo numero di cicli necessari per raggiungere quella dimensione della cricca
%% calcolo come varia la dimensione della cricca al crescere del numero di cicli

a_fin = a_cr;

Nf = (a_fin^(1-(m/2)) - a_in^(1-(m/2)))/(C*(1-(m/2))*(sigma_max^m)*(pi^(m/2)));

N = 1 : 250: Nf;
```

```
a_N = (a_in^(1-(m/2))+ (C*(1-(m/2))*(sigma_max^m)*(pi^(m/2))*N)).^(1/(1-(
    m/2)));
a_N_prov = (a_in^(1-(m/2))+ (C*(1-(m/2))*(sigma_max^m)*(pi^(m/2))*33700))
    .^(1/(1-(m/2)));

dadN = @(N,a) C*(sigma_max*...
    (1 + 0.256*(a_cr /W) - 1.152 * (a_cr/W)^2 + 12.2*(a_cr/W)^3)*...
    ((pi*a)^0.5))^m;


Nff = 2.5e4;
options = odeset('Events', @myevent);  % Use the correct event function
    handle

% Solve the ODE with event function
[N_v, a_v, N_e, a_e, i_e] = ode45(dadN, [0 Nff], a_in, options);
```

2.3.3 Comparison of Different Materials

The same geometry and loading conditions as the previous exercises are still considered. Three different aluminum alloys are considered:

- 2024-T3 Al alloy with properties already shown in Fig.2.7
- 5083-O Al alloy, Fig.2.12
- 6061-T6 Al alloy, Fig.2.13
- 7075-T6 Al alloy, Fig.2.14

.

The crack growth and propagation rate curves obtained with the NASGROW model using AFGROW software are compared. The final values of the crack, Y, and K for each alloy are also shown. In particular, it is observed that: the fatigue life of the 2024-T3 alloy is by far the highest, and for this reason, it is almost always used for the ventral panels of the wing. The 7075-T6 Al alloy, on the other hand, is more often used for the dorsal panels because it has high compressive limit load values.

Property	Value	Property Description
E	71016	Young's Modulus
Nu	0.33	Poisson's Ratio
AlphaT	2.38e-005	Coefficient of thermal expansion
UTS	43	Ultimate tensile strength
YS	137.895	Yield stress
K1e	69.227	Effective fracture toughness for surface/elliptica...
K1c	49.448	Plane strain fracture toughness
Ak	1	Fit Parameter
Bk	0.1	Fit Parameter
Rlo	-0.3	Negative cut-off stress ratio
Rhi	0.7	Positive cut-off stress ratio
C	5.2687e-...	Paris crack growth rate constant
n	1.938	Paris exponent in Forman-Newman-de Koning-H...
p	0.5	Exponent in Forman-Newman-de Koning-Henrik...
q	1	Exponent in Forman-Newman-de Koning-Henrik...
DKo	5.494	Threshold stress intensity factor range at R = 0
Cth	2	Threshold coefficient
Alpha	1.5	Plane stress/strain constraint factor
Smax/SIGo	0.3	Ratio of the maximum applied stress to the flow ...

Figure 2.12 Properties of 5083-O Al alloy

Property	Value	Property Description
E	68947.6	Young's Modulus
Nu	0.33	Poisson's Ratio
AlphaT	2.36e-005	Coefficient of thermal expansion
UTS	45	Ultimate tensile strength
YS	282.685	Yield stress
K1e	39.558	Effective fracture toughness for surface/elliptica...
K1c	28.57	Plane strain fracture toughness
Ak	1	Fit Parameter
Bk	0.75	Fit Parameter
Rlo	-0.3	Negative cut-off stress ratio
Rhi	0.7	Positive cut-off stress ratio
C	1.8404e-...	Paris crack growth rate constant
n	2.3	Paris exponent in Forman-Newman-de Koning-H...
p	0.5	Exponent in Forman-Newman-de Koning-Henrik...
q	0.5	Exponent in Forman-Newman-de Koning-Henrik...
DKo	3.846	Threshold stress intensity factor range at R = 0
Cth	1.5	Threshold coefficient
Alpha	2	Plane stress/strain constraint factor
Smax/SIGo	0.3	Ratio of the maximum applied stress to the flow ...

Figure 2.13 Properties of 6061-T6 Al alloy

Property	Value	Property Description
E	71705.5	Young's Modulus
Nu	0.33	Poisson's Ratio
AlphaT	2.36e-005	Coefficient of thermal expansion
UTS	84	Ultimate tensile strength
YS	517.107	Yield stress
K1e	40.657	Effective fracture toughness for surface/elliptica...
K1c	29.669	Plane strain fracture toughness
Ak	1	Fit Parameter
Bk	1	Fit Parameter
Rlo	-0.3	Negative cut-off stress ratio
Rhi	0.7	Positive cut-off stress ratio
C	4.0211e-...	Paris crack growth rate constant
n	2.947	Paris exponent in Forman-Newman-de Koning-H...
p	0.5	Exponent in Forman-Newman-de Koning-Henrik...
q	1	Exponent in Forman-Newman-de Koning-Henrik...
DKo	3.297	Threshold stress intensity factor range at R = 0
Cth	2	Threshold coefficient
Alpha	1.9	Plane stress/strain constraint factor
Smax/SIGo	0.3	Ratio of the maximum applied stress to the flow ...

Figure 2.14 Properties of 7075-T6 Al alloy

```
*********Fracture based on ' Kmax' Criteria (current maximum stress)
 C  Crack size=  0.22116  Beta= 1.1380  R(k)= 0.0000  R(final)= 0.0000   Delta k=7.5885e+001   D()/DN=2.5400e-003
Max stress =    80.000  r =  0.00     157302  Cycles  Constant amp.:     1574   Pass:  1574
```

Figure 2.15 Results for 2024-T3 Al alloy

```
*********Fracture based on ' Kmax' Criteria (current maximum stress)
 C  Crack size=  0.13808  Beta= 1.0482  R(k)= 0.0000  R(final)= 0.0000   Delta k=5.5229e+001   D()/DN=2.5400e-003
Max stress =    80.000  r =  0.00      83796  Cycles  Constant amp.:      838   Pass:  838
```

Figure 2.16 Results for 5083-O Al alloy

```
*********Fracture based on ' Kmax' Criteria (current maximum stress)
 C  Crack size=  0.11685  Beta= 1.0339  R(k)= 0.0000  R(final)= 0.0000   Delta k=5.0112e+001  D()/DN=2.5400e-003
Max stress =    80.000  r =  0.00      89500  Cycles  Constant amp.:      896  Pass:  896
```

Figure 2.17 Results for 6061-T6 Al alloy

```
*********Fracture based on ' Kmax' Criteria (current maximum stress)
 C  Crack size=  0.15777  Beta= 1.0642  R(k)= 0.0000  R(final)= 0.0000   Delta k=5.9936e+001  D()/DN=2.5400e-003
Max stress =    80.000  r =  0.00      86076  Cycles  Constant amp.:      861  Pass:  861
```

Figure 2.18 Results for 7075-T6 Al alloy

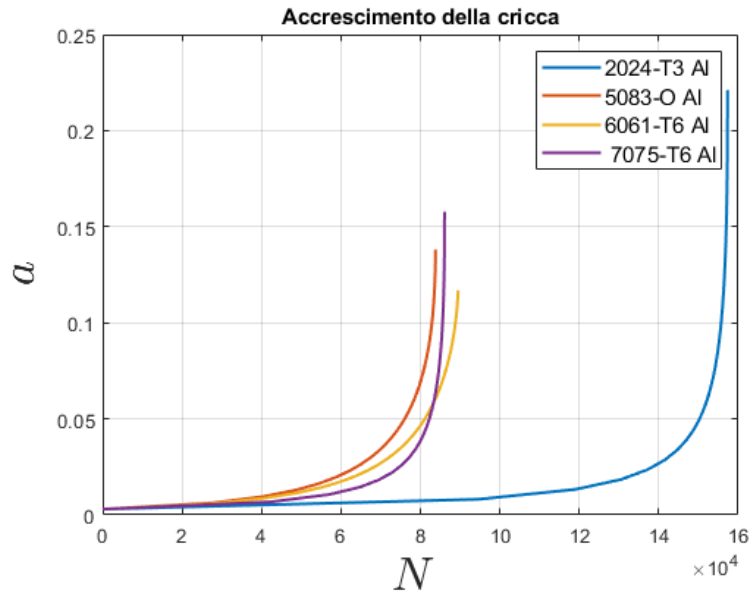

Figure 2.19 Crack growth with the number of cycles for different alloys

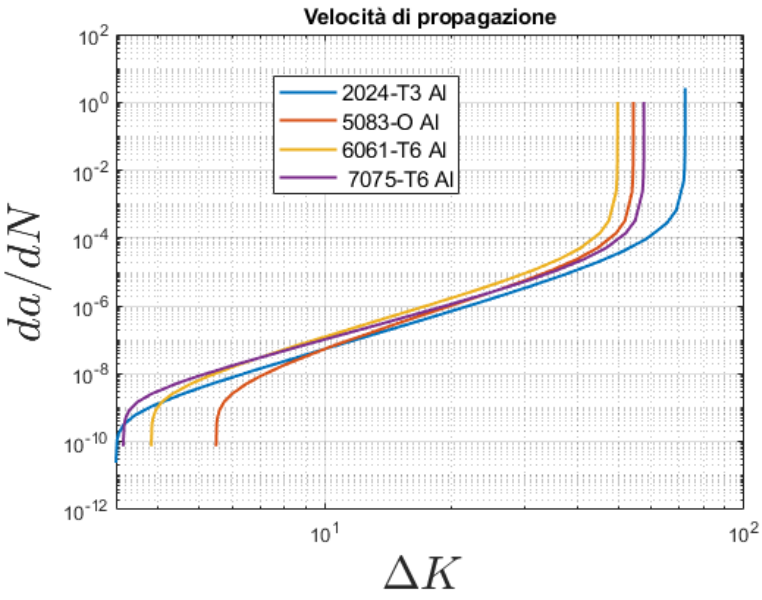

Figure 2.20 Propagation rate for different alloys

2.3.4 Effect of the Presence of a Hole

The plate from the previous exercises is considered, with the same load spectrum and the material being 2024-T3 Al alloy. This time, the effect of the presence of a hole is evaluated. In particular, different hole radii are considered. The results in Fig.2.21-Fig.2.27 show that:

- The presence of a hole near the crack always leads to a higher critical crack size.
- The number of cycles to failure changes significantly with the dimensions of the hole diameter (D).
- It is particularly observed that the presence of a hole much smaller than the initial crack size leads to a much higher number of load cycles to failure compared to the case without a hole. This phenomenon can be explained by considering the expression of the stress concentration factor (Eq.2.1). The presence of the hole at the apex is as if it increases the 'b' dimension of the crack and consequently reduces the local stress values. As a result, the crack propagates more slowly.
- High values of the hole diameter compared to the initial crack size lead to much lower values of cycles to failure. If the hole is very large, it diverts the stress flow lines and leads to an overall increase in stress around the crack, which then propagates very quickly.
- The presence of a hole slightly larger than or comparable to the initial crack size does not significantly change the value of the cycles to failure.
- It is also observed that as the hole size increases, not only does the number of cycles to failure decrease, but the critical crack size also decreases.

```
**********Fracture based on ' Kmax' Criteria (current maximum stress)
 C  Crack size=  0.35498 Beta= 0.8778 R(k)= 0.0000 R(final)= 0.0000   Delta k=7.4162e+001  D()/DN=2.5400e-003
Max stress =   80.000  r = 0.00    573729  Cycles  Constant amp.:     5738  Pass:  5738
```

Figure 2.21 Results for hole diameter D=0.00006 m

```
**********Fracture based on ' Kmax' Criteria (current maximum stress)
 C  Crack size=  0.3514 Beta= 0.8724 R(k)= 0.0000 R(final)= 0.0000   Delta k=7.3332e+001  D()/DN=2.5400e-003
Max stress =   80.000  r = 0.00    488678  Cycles  Constant amp.:     4887  Pass:  4887
```

Figure 2.22 Results for hole diameter D=0.0006 m

```
**********Fracture based on ' Kmax' Criteria (current maximum stress)
 C  Crack size=  0.34482 Beta= 0.8741 R(k)= 0.0000 R(final)= 0.0000   Delta k=7.2778e+001  D()/DN=2.5400e-003
Max stress =   80.000  r = 0.00    198983  Cycles  Constant amp.:     1990  Pass:  1990
```

Figure 2.23 Results for hole diameter D=0.006 m

```
*********Fracture based on ' Kmax' Criteria (current maximum stress)
 C  Crack size=   0.3419  Beta= 0.8840  R(k)= 0.0000  R(final)= 0.0000   Delta k=7.3292e+001   D()/DN=2.5400e-003
Max stress =    80.000   r =  0.00     118073  Cycles  Constant amp.:     1181   Pass:  1181
```

Figure 2.24 Results for hole diameter D=0.012 m

```
*********Fracture based on ' Kmax' Criteria (current maximum stress)
 C  Crack size=   0.30636  Beta= 0.9485  R(k)= 0.0000  R(final)= 0.0000   Delta k=7.4444e+001   D()/DN=2.5400e-003
Max stress =    80.000   r =  0.00     22140  Cycles  Constant amp.:     222   Pass:  222
```

Figure 2.25 Results for hole diameter D=0.06 m

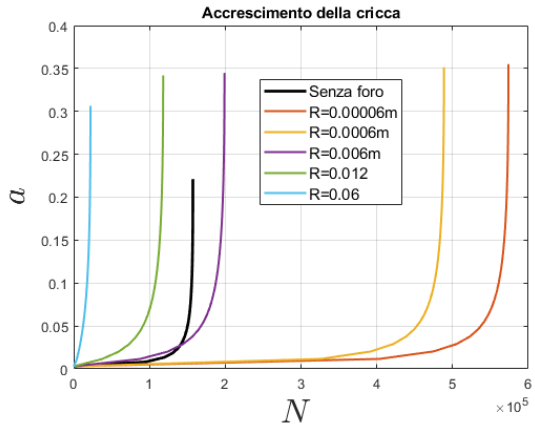

Figure 2.26 Comparison of crack growth trends for a plate without a hole and with holes of different sizes

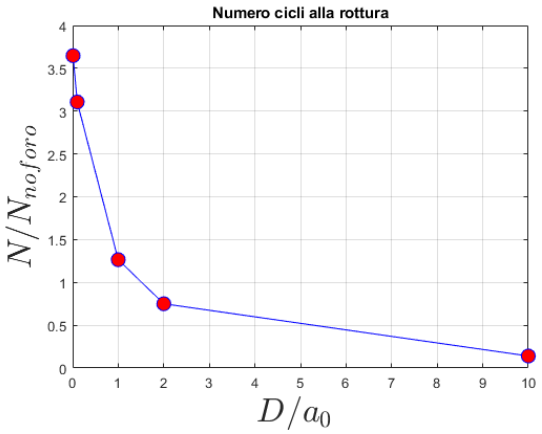

Figure 2.27 Number of cycles to failure relative to the number of cycles to failure for an unnotched plate, as a function of the hole diameter dimension relative to the initial crack size

2.3.5 Repair with Composite Patch

To slow down crack propagation, repair with a composite material patch is often used. The patch is bonded to the plate at the crack location, thereby reducing the stresses around the crack. This happens because part of the stresses pass through the patch. In particular, it is also observed that the greater the stiffness of the patch, the greater the amount of stress absorbed by it. However, increasing the patch stiffness does not necessarily lead to better results because what can occur with excessively high stiffnesses

is that the stress causes a failure of the adhesive, and consequently, the patch cannot perform its intended function. In this section, the same plate from the previous sections (with 2024-T3 Al material) is studied, and the effect of repair with a composite patch is investigated. The chosen composite material is Graphite/Epoxy BMS 8-212 Type II Class 1, already seen in previous chapters, with properties shown in Table 2.3.

Property	**Value**
E_1	125 GPa
E_2	12.5 GPa
G_{12}	6.89 GPa
ν_{12}	0.38
ν_{21}	0.038

Table 2.3 Material properties

The symmetric sequence $[\pm 45°/\ 0°/\ 0°/\ 0°/\ 90°]$ and a thickness per ply of 0.15 mm were considered. AFGROW software was used for the analyses, and the results for different patch widths W_p are reported. In particular, it is observed that the presence of the patch, as expected, greatly increases the fatigue life of the plate. Furthermore, it is trivially observed that the larger the patch size, the greater the number of cycles to failure.

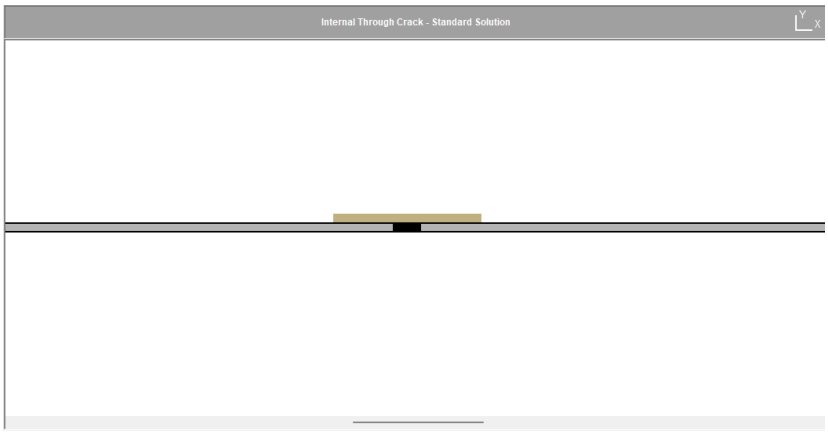

Figure 2.28 Repair with Composite Patch

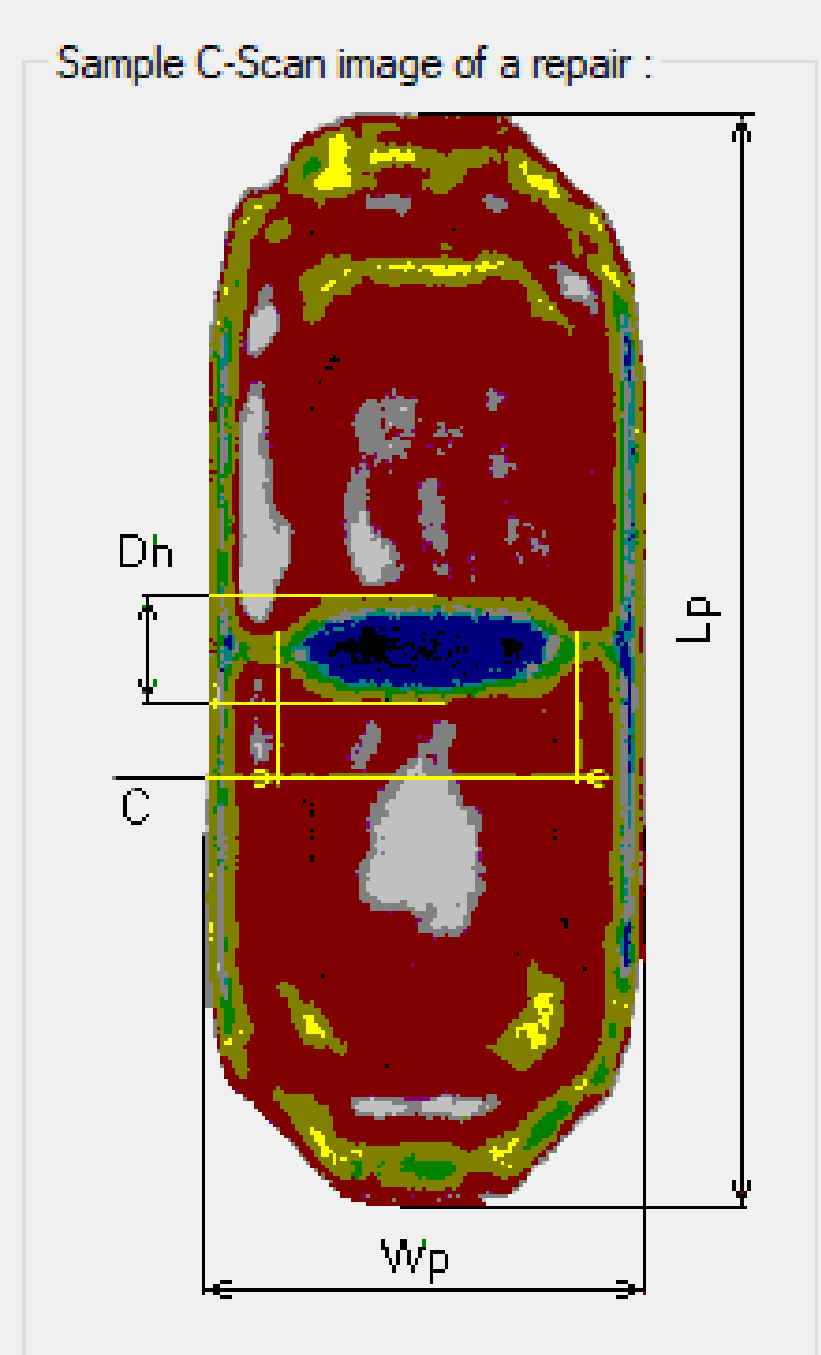

Figure 2.29 Composite Patch

C Crack size= 0.38866 Beta= 0.4314 R(k)= 0.0000 R(final)= 0.0000 Delta k=3.8132e+001 D()/DN=9.3299e-006
Max stress = 80.000 r = 0.00 3512300 Cycles Constant amp.: 35124 Pass: 35124

Figure 2.30 Results with Patch width W_p=1m

********Fracture based on ' Net Section Yield' Criteria (current maximum stress)
C Crack size= 0.38998 Beta= 0.5423 R(k)= 0.0000 R(final)= 0.0000 Delta k=4.8018e+001 D()/DN=2.8255e-005
Max stress = 80.000 r = 0.00 2156200 Cycles Constant amp.: 21563 Pass: 21563

Figure 2.31 Results with Patch width W_p=0.3m

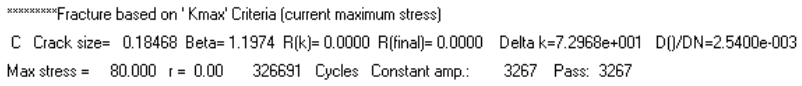

Figure 2.32 Results with Patch width W_p=0.03m

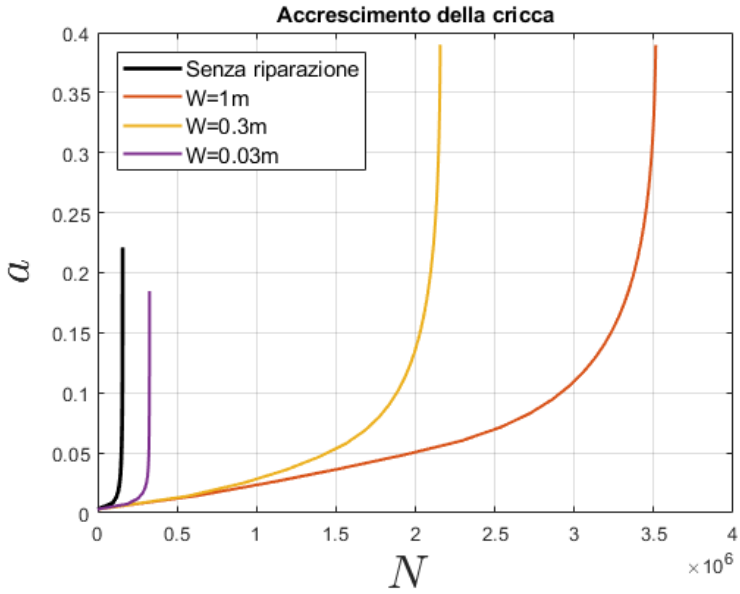

Figure 2.33 Comparison of repair effect for different widths with the unrepaired case

2.3.6 Order of Load Application

So far, we have always considered the same sinusoidal load spectrum with a minimum value $\sigma_{min} = 0$ and maximum value $\sigma_{max} = 0$. Now we want to evaluate if AFGROW implements an algorithm that considers the effect of the order in which loads are applied on fatigue life. It was decided to consider load spectra with three different amplitude values (10 MPa, 50 MPa, 80 MPa). For the medium amplitude load, a very high number of cycles was chosen to ensure fatigue failure before the end of the spectrum application itself. This ensures that the different results will not be influenced by different numbers of cycles for the different components (the number of cycles associated with the smallest load and that associated with the largest load are fixed). For both load spectra in Figs.2.34-2.35, the result in Fig.2.36 was obtained, while for the load in Fig.2.37, the result in Fig.2.38 was obtained. It is observed that the results do not vary at all for the first 2 spectra. This would lead to the conclusion that there is no dependence of the results on the order of load application. The variation, albeit minimal, encountered in the last sequence could be associated with numerical errors in the integration of the NASGROW equation.

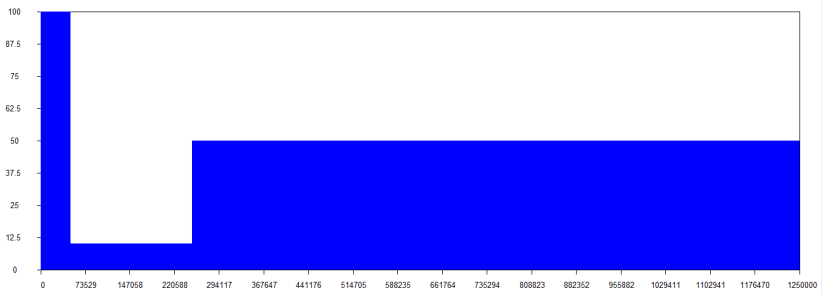

Figure 2.34 Spectrum with largest component then smallest, then medium

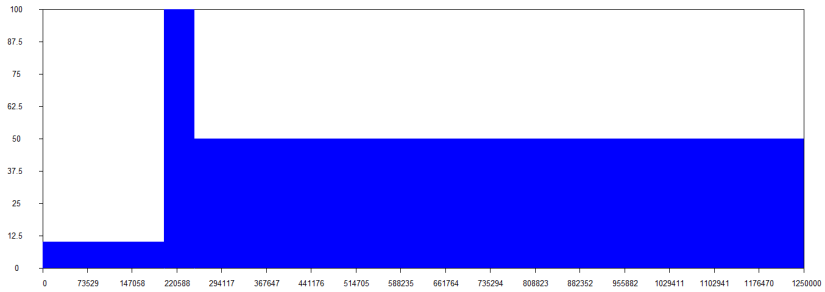

Figure 2.35 Spectrum with smallest component, then largest, then medium

```
********Fracture based on ' Kmax' Criteria (current maximum stress)
 C  Crack size=  0.33817  Beta= 1.4349  R(k)= 0.0000  R(final)= 0.0000   Delta k=7.3949e+001  D()/DN=2.5400e-003
Max stress =   50.000  r =  0.00     555457  Cycles     Label:        1   Pass:    1
```

Figure 2.36 Result for the two spectra

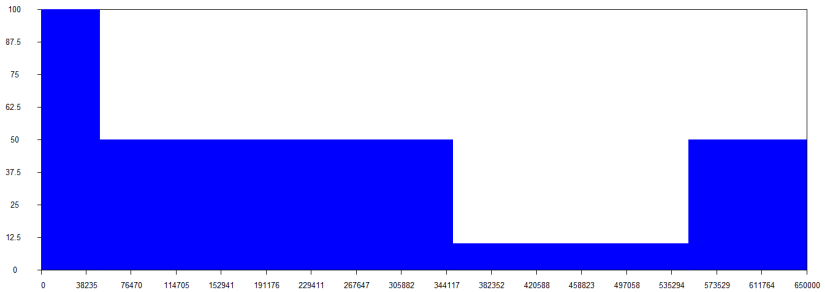

Figure 2.37 Spectrum with high, medium, low, medium components

```
********Fracture based on ' Kmax' Criteria (current maximum stress)
 C  Crack size=  0.3411  Beta= 1.4473  R(k)= 0.0000  R(final)= 0.0000   Delta k=7.4909e+001  D()/DN=2.5400e-003
Max stress =   50.000  r =  0.00     555017  Cycles     Label:        1   Pass:    1
```

Figure 2.38 Result for the last spectrum